Reviews in Mineralogy & Geochemistry
Vol. 84 pp. 57–83, 2018

Molecular Clusters and Solvation in Volcanic and Hydrothermal Vapors

Kono H. Lemke

Department of Earth Sciences
University of Hong Kong
Pokfulam Road
Hong Kong SAR
China

Terry M. Seward

SGEES
Victoria University of Wellington
Wellington 6140
New Zealand

INTRODUCTION

Throughout the Earth's crust from magmatic/volcanic to lower temperature hydrothermal environments, low density aqueous fluids play a fundamental role in its chemical evolution. These gas-like fluids contain a periodic table of elements but their molecular chemistry has been little studied. Even the gas-phase molecular chemistry of the solvent itself, steam or low density supercritical water, is poorly known. These low density, gas-like aqueous fluids are important reactive, chemical transport media (Henley and Seward 2018, this volume) throughout the crust and may exit into the Earth's ocean–atmosphere system, contributing to ocean and atmospheric chemistry throughout geologic time. The importance of high temperature gas–solid reactions in crustal evolution and ore deposit formation has recently been emphasized by Henley et al. (2017) in their study of the enormous skarn deposits associated with the giant Grasberg porphyry deposit at Ertsberg in Indonesia.

Low-density water solvent (steam or water vapor) at elevated temperatures is not a hydrogen bonded dielectric continuum as is liquid water at temperatures above about 150 °C (see for example Seward and Driesner 2004, and references therein). Water vapor is comprised of aggregates of waters molecules held together by hydrogen bonding with the cluster sizes and geometries defined by the water gas density (or pressure) at a given temperature. We present new data on the size, energetics (stabilities) and geometries of molecular water clusters in water vapor as well as data on the solvation of both ionic and molecular species in the water cluster environment. We discuss the solvation of the proton, or more correctly, the hydrated proton, by water clusters, which comprise the basis for our understanding of pH and the equilibrium ion product constant, K_w, of water vapor. The solvation of a number of dissolved species relevant to high temperature natural systems, including NaCl, H_2S and HS^- is also discussed. We also present new data on the cluster solvation of Au^+ as well as the simple monochloridogold(I) complex, $AuCl^\circ$, in water vapor at elevated temperatures. These observations provide fundamental molecular insight into the reactivity and transport chemistry of high temperature water vapor in the Earth´s crust but our observations are only a reconnaissance because so little is known.

1529-6466/18/0084-0002$05.00 (print)
1943-6266/18/0084-0002$05.00 (online)
http://dx.doi.org/10.2138/rmg.2018.84.02

The topic of gas-phase (molecular and ionic) chemistry is a relatively new and an exciting domain of research in the Earth Sciences. Despite being a new field of geochemistry, it has attracted considerable attention, from both within and outside the Earth Sciences, by the experimental community (Casey and Swaddle 2003; Casey and Rustad 2007) and now increasingly from the theoretical chemistry community (Zhao and Truhlar 2010). Research on gas-phase ions over the past three decades has opened up exciting new possibilities for geochemists to examine the structure and stability of solvated gaseous ions, which makes it possible to understand why gaseous ions behave fundamentally differently from their bulk (liquid) analogues, and distinguish between intrinsic properties of ion(-molecule) clusters and properties resulting from their solvation environment. For example, the concept of vapor pH is directly linked to the formation of solvated proton clusters (or hydroxide water clusters), that exist with fundamentally different bonding motifs (see Fig. 1), i.e. Eigen vs Zundel, exterior vs interior ion positions, and dynamically transform as the solvation shell grows and evolves from cluster-size towards structures with bulk-like environments

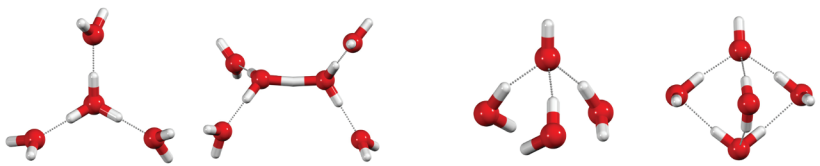

Figure 1. Structures of protonated Eigen and Zundel water cluster ions, and hydroxide water clusters with first and second shell water solvation.

Probing solvated ion clusters using mass spectrometry, and more recently, in combination with structure-sensitive infrared (IR) spectroscopic techniques, has helped to reveal the nature of ion-water interactions in gas-phase clusters (Robertson and Johnson 2003). For example, the solvation of the hydroxide ion in water vapor stands out as an interesting case where completion of the first solvation shell with $OH^-(H_2O)_3$ and emergence of a second solvation shell in $OH^-(H_2O)_4$ is marked by changes in IR bands caused by inter-water hydrogen bonding (Robertson et al 2003). Interestingly, solvated fluoride anions display comparable spectral shifts as the solvation shell evolves to include a strongly bound water–water network beginning in $F^-(H_2O)_5$ with spectral features typical of internally solvated ions. Larger halide ions such as Cl^-, Br^- and I^-, on the other hand, display IR spectral features characteristic of surface-solvated ions, in other words, the primary solvation shell is only partially filled with the halide ion positioned at the water cluster surface (e.g. Robertson and Johnson 2003; Likhoyot et al. 2005). We will later see that these solvation motifs play a key role in the positioning of ions at water–vapor interfaces, with important implications for the partitioning of molecular ions across phase boundaries during film, bubble and droplet formation in high temperature vapor.

The experimental study of gaseous ions provides obvious advantages over bulk phase studies, because the former can resolve spectroscopic signatures that stem from single, double and higher-order ion aggregates whereas solution phase methods often yield averaged signals and rarely provide direct evidence for ion clustering. However, ion cluster studies are also attended by challenges, and these are predominantly due to trade-offs as to how mass spectrometric facilities are linked to laser spectroscopic systems, but also the role that ambient blackbody radiation has on the stability of a cluster. There are some exciting new developments in cryogenically cooled mass spectrometers that will overcome some of these difficulties and permit the probing of cluster structures as a function of temperature (Guo et al. 2004). The past decade has seen an explosion

in the number of mass spectrometric/IR laser spectroscopic investigations of solvated molecular ions, and this is in part due to recent developments in tunable optical parametric oscillator/amplifier (OPO/OPA) laser systems and a growing number of mass spectrometric facilities with mass selection and storage capabilities, such as time-of-flight (TOF-MS) and Fourier-transform ion cyclotron resonance (FT-ICR-MS) mass spectrometry.

The challenge of transferring molecular ions from the solution into the gas-phase, without causing any significant changes to the molecular structure and distribution, has been addressed by probing concentration and pH-dependent changes in ion cluster populations following electrospray ionization (Schröder et al. 2011, Schröder 2012). From a computational perspective, larger clusters ($>80\,H_2O$) have been intractable using reliable high level theory, primarily because of their size and configurational complexity, but also because these systems require appropriate theory to accurately describe interactions ranging from relativistically driven metal-metal bonding to dispersion dominated weak interactions in the solvation shell (Zhao et al. 2006; Zhao and Truhlar 2008, 2010). Consequently, density functional theory (DFT) with continuum methods (PCM), and explicit first shell solvation, are the work-horse methods used in most simulations of microsolvated clusters, however, scattered evidence indicates that this approach is impractical and often fails to predict the correct properties for solvated ion clusters. Some of these problems are now being overcome, such as for instance, finding the global minimum of a solvated (>50 waters) ion cluster which is still a formidable task but can be achieved using artificial bee colony (Zhang and Dolg 2016), basin hopping type optimizations (Wales et al. 2007) and genetic algorithm based techniques (Schulz and Hartke 2002).

The main focus of this review is on the gas-phase physical geochemistry of single ions, ion pairs and polynuclear ions solvated with geochemically relevant molecules (e.g. H_2O, NH_3, H_2S, CO_2 etc.) using insights from mass spectrometry (e.g. FT-ICR-MS) and vibrational spectroscopy with tunable IR laser sources. The combination of FT-MS and IR spectroscopy can provide valuable information on the structure of the ion core and solvation shell; however, this approach entails several challenges, in particular the ability to control the temperature in the vicinity of the ion detector/ICR cell still remains an obstacle. Ions with large solvation shells generally require cryogenic cooling, and thus, if these ions are exposed to a controlled blackbody field generated within the mass spectrometer, IR spectra can be obtained for mass-selected ions with temperature-dependent solvation shell structures. Other mass spectrometric techniques, such as HPMS, complement FT-ICR MS IRMPD measurements and provide important thermodynamic information on the interaction of solvent molecules with ions (Meot-Ner 2005, and refs. therein).

The interpretation of mass spectrometric and IRMPD spectra builds critically on results from molecular simulations, and this task becomes increasingly challenging as the size of the cluster increases. This problem is further compounded when inter-water hydrogen bonding in the solvation shell around an ion gives rise to closely spaced (<5–$10\,cm^{-1}$) IR absorption bands and band broadening effects, comparable to those of liquid water (Robertson et al. 2003; Headrick et al. 2005). The traditional approach so far has been through DFT frequency modeling with unique scaling factors, but this approach very often fails to reproduce complex IR spectra (and at best provides the right answer for the wrong reason). Alternative variants of density functional theory, e.g. DFT-D*n*, M0X-2X and PBE-D, designed specifically for weakly bound systems (i.e. bound by hydrogen bonding, weak electrostatic and dispersion-type interactions, e.g. see Lemke and Seward 2013; Lemke 2014a), second-order vibrational perturbation theory (VPT2) (Barone 2004) and *n*-split frequency scaling strategies (Temelso and Shields 2011), which have emerged over the last decade provide new and robust, albeit expensive, means of interpreting complex vibrational spectra for molecular clusters.

We therefore begin our discussion of molecular clusters with a brief overview of neutral water clusters and complete the review describing ongoing research into ionic and molecular

clusters that are examined with a focus on their behavior in vapor-like fluids. For pure water clusters, the emphasis in this review lies on the spectroscopic and theoretical examination of their structures and energies. Results from novel laser spectroscopic methods in combination with second-order Møller-Plesset (MP2) and coupled cluster CCSD(T) level calculations have helped to elucidate the molecular details of a wide range of isomers of small (n=6–10) (Huisken et al. 1996; Buck et al. 1998, Keutsch and Saykally 2001) and medium-sized (n>10) water clusters (Pradzynski et al. 2012). These findings are crucial for understanding droplet nucleation phenomena in water vapor, aerosols, clouds and atmospheric chemistry processes occurring at the nanodroplet interior and surfaces.

THE MOLECULAR STRUCTURE OF WATER VAPOR (STEAM AND LOW DENSITY SUPERCRITICAL WATER)

Neutral Clusters

The dimer and small ring structures: The first experimental account of the water dimer, $(H_2O)_2$, dates back to 1957 and reported OH-stretching and bending vibrations in the 1600–3500 cm^{-1} spectral region using cryogenic matrices (Van Thiel et al. 1957). Subsequent IR spectroscopic (Liu et al. 1996a; Braly et al. 2000a,b), thermal conductivity (Curtiss and Blander 1979, 1988) and quantum chemical studies (Xantheas 1994; Feyereisen et al. 1996; Xantheas et al. 2002; Lemke and Seward 2008a, Mukhopadhyay et al. 2018, and refs therein) of $(H_2O)_2$ (and smaller water clusters) have yielded valuable insight into the structure and stability of the simple dimer, and as of this review, there are around 1700 publications that have examined the water dimer both experimentally and theoretically. Figure 2 below presents a van't Hoff plot for the water clustering reaction $(H_2O)_n+(H_2O)=(H_2O)_{n+1}$ generating ring-type $(H_2O)_3$ (2,3), $(H_2O)_4$ (3,4) and $(H_2O)_5$ (4,5) clusters and these results have been obtained at the CCSD(T)/CBS limit level of theory.

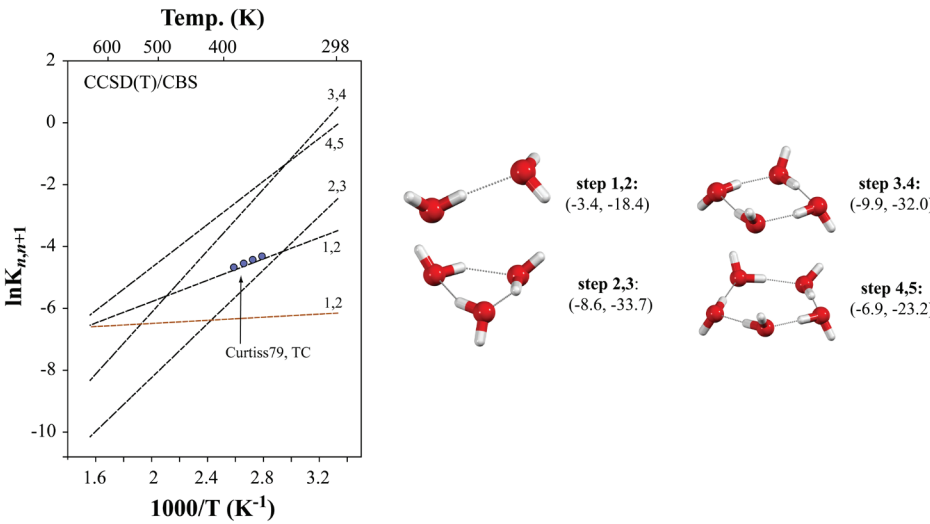

Figure 2. left: Van't Hoff plot for $(H_2O)_n$ + (H_2O) = $(H_2O)_{n+1}$ clustering reaction together with equilibrium thermal conductivity (TC) measurements for water dimerization (1,2) reaction (Curtiss 1979). **right:** water cluster geometries and CCSD(T)/CBS level stepwise clustering enthalpies (kcal/mol) and entropies (cal/mol/K) shown in brackets. Also shown for reference are data for the H_2S dimer (brown) taken from Lemke (2017).

Given the importance of smaller water clusters, it seems appropriate to briefly comment on the thermodynamic properties of these species. In Figure 2, values for the stepwise water clustering equilibria are shown as a function of temperature from 298 K up to ~640 K, and it is seen that all clustering reactions exhibit positive slopes (i.e. negative clustering enthalpies) over the full temperature range, corresponding to a decrease in cluster stability with increasing temperature. The magnitude of this decrease in stability, however, differs from cluster to cluster, indicating, for instance, that the water dimer would play a more significant role as a molecular species in water vapor at higher temperatures, whereas higher clusters would undergo full dissociation to their constituent monomers and play a less important role in water vapor. In fact, Slanina and coworkers (Slanina 1988; Slanina et al. 2006) have examined temperature effects for several water clustering equilibria and concluded that water clusters disassociate with increasing temperature, in particular at hydrothermal temperatures. It was also noted that water clusters would play a more important role in low-temperature saturated vapor over ice or liquid water, given the increasing thermodynamic favor for water clustering at lower temperatures. However, because water vapor pressures are significantly higher along the two phase curve, particularly in the vicinity of the critical point of water, a large fraction of the monomer population will likely interconvert to the water dimer and larger clusters. In Figure 3 below, the partial pressures of water clusters with $n=2$–4 are presented as a function of temperature for vapor saturation conditions.

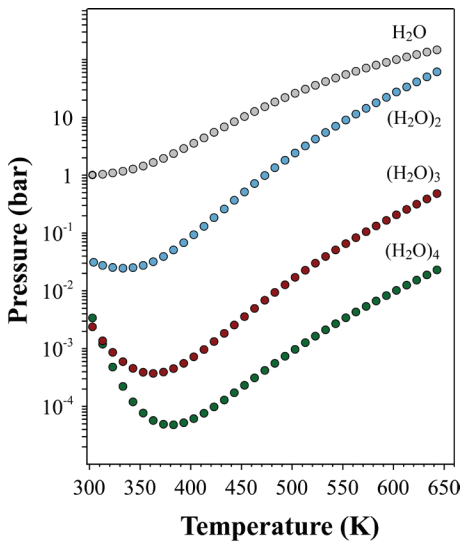

Figure 3. Abundance profiles of water clusters $(H_2O)_n$ with $n=2$–4 in equilibrium with H_2O (liquid) along the liquid–vapor phase boundary from 298 to 646 K. Note the initial dip in cluster abundance at lower temperatures, inflection at 350 ($n=2$), 360 ($n=3$) and 380 K ($n=4$) followed by a steady increase in water cluster abundance with increasing temperature up to the critical region.

Our calculations demonstrate that the (exponentially) increasing water monomer pressure along the liquid vapor phase boundary suffices to enhance the stability of water clusters, in particular, in the case of the water dimer; results from CCSD(T)/aVTZ calculations predict that approximately 40% of the vapor phase is composed of water dimers, with noticeable contributions from $(H_2O)_3$ and $(H_2O)_4$ that steadily increase with increasing temperature; it is also worth noting that our predicted levels of trimer and tetramer clusters are not necessarily a good diagnostic for the abundance of larger clusters in water vapor because water cluster beginning with $n>6$ form three-dimensional structures that possess higher stabilities compared with ring-like $(H_2O)_3$, $(H_2O)_4$ and $(H_2O)_5$. Cluster structures that so far have not been examined for their ability to exist in ambient over even high-temperature aqueous vapors, in spite of their well-known stability, include compact $(H_2O)_6$ species and as discussed further below, cubic $(H_2O)_8$ and the magic number dodecahedral $(H_2O)_{20}$ clusters.

Medium sized water clusters, n = 4–10. Saykally and coworkers (Pugliano and Saykally 1992; Cruzan et al. 1996; Liu et al. 1996a,b,c; Gregory et al. 1997) reported the first account of the structure and spectra of the larger water clusters $(H_2O)_n$ with $n = 3–6$, using far-IR vibrational-tunneling (VRT) spectroscopy. Huisken et al. (1996) subsequently reported the first experiments to observe water OH-stretching bands in $(H_2O)_n$ ($n = 3–5$) by recording infrared predissociation (IRPD) spectra in the spectral region 3300–3800 cm^{-1} of mass-selected water clusters. These studies were followed up by an experimental investigation of the three-dimensional forms of $(H_2O)_6$ by Saykally and coworkers (Liu et al. 1996a). Several important points evolve from these studies which show that the lowest energy conformers of the water hexamer adopt three-dimensional structures (e.g. prisms, cages, books, boats, etc). However, smaller water clusters ($n = 2–5$) maintain linear or cyclic configurations, and the stability ranking of the five lowest-energy $(H_2O)_6$ structures changes when vibrational zero-point energies are taken into account; i.e. the cage configuration of $(H_2O)_6$ is favored over the prism form when ZPE effects are considered. Buck et al. (1998) measured the first IR predissociation spectra for larger water clusters $(H_2O)_n$ ($n = 8–10$) using supersonic expansion techniques, vibrational predissociation spectroscopy and theoretical MP2/DZP calculations and found that $(H_2O)_{8–10}$ adopt microcrystalline structures based on small water octamers in which water molecules occupy the vertices of a cube. The most stable water nonamer ($n = 9$) and decamer ($n = 10$) structures, on the other hand, are derived from cubic $(H_2O)_8$ by insertion of one and two two-coordinated molecules into the cube edges. Therefore one might expect that IRMPD fingerprint spectra of $(H_2O)_9$ and $(H_2O)_{10}$ to retain features of the cubic octamer, while also showing characteristic red-shifted OH-stretching bands associated with these "newly" inserted singly and doubly coordinated water molecules.

Figure 4 shows an example of IR-predissociation spectra (Buck and Huisken 2000) of water clusters having $n = 7–20$ as well as the IR absorption spectrum of liquid water at 298 K;

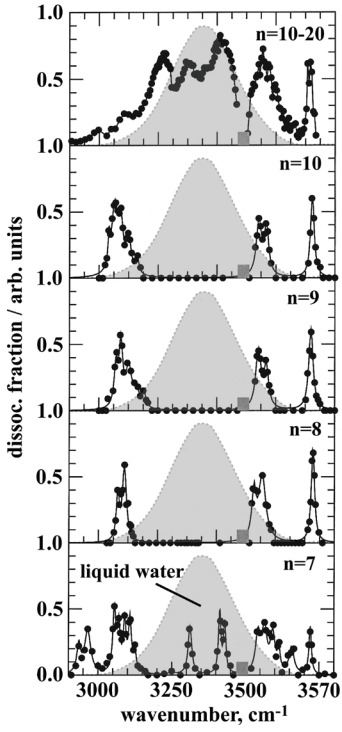

Figure 4. IR photo dissociation (IRPD) spectra of mass-selected water clusters $(H_2O)_n$ with $n = 7–20$ in the OH stretching region (modified from Buck and Huisken 2000) together with the broad OH stretch band in ordinary liquid water at 298 K shown in grey (Maréchal 2011).

these data have been added to illustrate the breadth of the interwater OH-stretching bands in bulk water (Maréchal 2011). It may be seen that the octa-, nona- and decamer water clusters exhibit characteristic spectral bands around 3050–3150, 3550–3620 and 3720 cm^{-1}, and a large absorption gap exists from around 3200 to 3500 cm^{-1}. For the water octamer, the 3720 cm^{-1} spectral feature is assigned to free OH-stretching modes in water molecules at cube vertices, while broader features at 3050–3150 and 3550–3620 cm^{-1} are attributable to symmetric and asymmetric OH stretching modes of hydrogen-bonded water molecules, respectively; note, these are red-shifted by several hundred wavenumbers, relative to gas phase water. A comparison of experimentally measured OH vibrational spectra with reported *ab inito* results (Maeda and Ohno 2007) indicates that interactions in larger water clusters require dispersion sensitive ab initio theory, such as MP2, DFT-D*n* or M0X-2X functionals, in order to accurately reproduce the OH-stretching frequencies for $(H_2O)_{8–10}$ and in larger water clusters.

Large water clusters, n>10. Although a detailed discussion of larger ($n>10$) water cluster structures and energies is beyond the scope of this review, we provide an introductory overview of some of the key molecular features of larger water clusters with more than 10 water molecules. This is meaningful given the central role that size and structure have on physico-chemical properties (i.e. melting, boiling/condensation and critical points) of water clusters and nanodroplets (Johnston and Molinero 2012). More recently, water clusters and nanodroplets have received growing interest from atmospheric chemists due to cluster surface–interior transfer processes of water molecules (Jungwirth and Tobias 2006; Buch et al. 2007). These structural transitions from an all-surface configuration where all water molecules reside at the cluster surface, to an interior configuration, where at least one fully solvated H_2O molecule exists inside a water cluster, play an important role in ion transfer processes between the cluster surface and interior. This structural transition, from all-surface to interior, is reported to occur at $n=17$ for water clusters, and has been predicted using CCSD(T)/aug-cc-pVTZ single point energies with MP2/aug-cc-pVTZ zero-point energy corrections (Yoo et al. 2010). A preliminary conclusion from these studies is that even high-level MP2 calculations are of insufficient accuracy to predict the energetic ordering among water clusters, such as $(H_2O)_{16}$ and $(H_2O)_{17}$, and instead, require costly CCSD(T) computations with triple-zeta size basis sets in order to successfully explore the potental energy surface (PES) of each cluster. This problem is further complicated due to the high number of isomeric forms that exist for $(H_2O)_{16}$ and $(H_2O)_{17}$; for example, both clusters have 500 distinct minima structures on the TIP4P PES, spanning an energy range of less than 20 kcal/mol. As noted in Yoo et al. (2010), the main theoretical problem lies in determining accurate energetic rankings for water clusters, and this task has proven to be extremely difficult due to the structural complexity and the exponentially increasing number of isomers that exist for larger water clusters. VRT- and IRPD-based spectroscopic methods have helped to identity water clusters up to the decamer, however, there are to the best of our knowledge, no experimental results available for $(H_2O)_n$ with $n>10$, with the exception of one study that reported IRMPD spectra for methanol-doped water clusters $(H_2O)_n(CH_3OH)$ with $n=15–20$ (Huisken et al. 1998). As a consequence, structural and energetic information for larger clusters are usually obtained using a combination of global optimization techniques and density functional methods.

Over the past decade, several new and promising approaches have been developed for resolving likely global minima water clusters structures. One such approach is the basin hopping/Monte Carlo minimization technique developed by Wales and coworkers (Wales and Hodges 1998; Wales and Scheraga 1999) in which the potential energy surface of water cluster are systematically explored using a Monte Carlo minimization approach in combination with pair potential functions. (e.g. for the TIP4P, TIP5P liquid water models, Mahoney and Jorgensen 2000). Alternative approaches to this problem include particle swarm optimization techniques (Lv et al. 2014), artificial bee colony (Zhang and Dolg 2016) and genetic algorithms (Guimarães et al. 2002), all of which have proven to provide valuable

insight into the nature of the potential energy surface of molecular clusters, and in a particular water cluster. Global minima structures of water clusters with up to 24 water molecules, which have been determined using an artificial bee colony algorithms in conjunction with the TIP4P water model as part of this review, are shown in Figure 5.

These optimization techniques, together with suitable DFT and MP2 computations, are among the most useful tools for water cluster structure determinations where spectroscopic data are not available, and, in particular, for large clusters with small energy differences among low-lying isomers. However, due to the mode of interaction and large number of isomers, computations of structures and energetic properties of larger water clusters is still a formidable task. For example, until recently, the nature of interactions and the complexity of the potential energy landscape led to the use of less accurate methods (B3LYP, PBE and BP86). This problem has in part been addressed following the introduction of new Minnesota DFT methods capable of modeling weak interaction in larger clusters, such M05–2X, M06–2X (Zhao et al. 2006) and the Grimme dispersion-sensitive functionals *m*PW2PLYP-D (Grimme 2006a), B2PLYP-D (Grimme 2006b) and B2PLYP-D3 (Grimme et al. 2011). Although these functionals can provide useful structural information and energetic trends, they very often fail to deliver reliable IR spectroscopic and thermodynamic properties because the intermolecular part of the PES in water clusters is typically anharmonic and cannot be accurately modeled with unique frequency scaling factors (Temelso and Shields 2011). The steady improvement in both HPC performance and implementation of faster ab inito methods, however, now permits structures and spectroscopic characterization of weakly bound water cluster systems, enabling global minima prediction for clusters with 20 water molecules with sub-kcal/mol accuracy (Yoo et al. 2010); this is achieved by using MP2 or coupled cluster theory CCSD(T). Correlation-based methods in conjunction with Dunning-style basis sets are the gold standard for water cluster simulations, and are capable of predicting individual vibrational modes (inter- and intramolecular) in small water clusters to within several wavenumbers (Howard et al. 2014). This approach however, becomes impractical for clusters with a large number of nearly

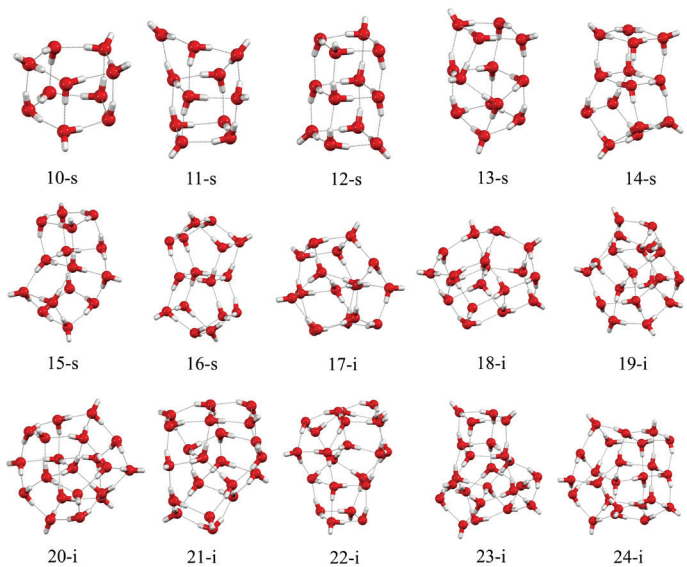

Figure 5. Equilibrium structures of water clusters $(H_2O)_n$ with $n = 10–24$ obtained from swarm optimization and M06–2X/aVDZ density functional calculations; note, 16-s is the largest all-surface species. i.e. all H_2O molecules reside on the cluster surface, and converts upon addition of H_2O, to an internally solvated cluster 17-I with interior water.

isoenergetic isomers because CCSD(T) calculations scale as N^7 with electron number and are prohibitively expensive relative to B97D, B2PLYP or even MP2 (both functionals employ MP2-like correlation that scale as N^5). For selected clusters, it is often possible to identify the global minimum configuration by comparing experimentally determined properties such as optical absorption, PES or IR vibrational spectra with those determined theoretically. For example, global minima structures of larger water clusters $(H_2O)_n$ with $n = 15–20$ are identified by comparing characteristic features of IR-predissociation spectra of methanol-doped water clusters $(H_2O)_n(CH_3OH)$ with MP2 IR spectroscopic simulations of water clusters in which the hydrogen-bonded methanol molecule at the cluster surface is replaced with a structurally equivalent water molecule (Buck and Huisken 2000; Jungwirth and Tobias 2006)

SOLVATION IN WATER VAPOR (SOLVATION IN AND ON NEUTRAL WATER CLUSTERS)

The hydrated proton and hydroxide ions

Magmatic and volcanic gases as well as steam produced by boiling in hydrothermal systems are low density aqueous media in which both ionic and molecular species are solvated ("dissolved") by water clusters, thus facilitating transport of volatile components such as SO_2, H_2S, CO_2, NH_3, N_2, NaCl as well as ionic species such as H_3O^+. Metal complexes are also stable in these low-density aqueous solutions which play a role in metal transport and deposition (ore deposits) in the Earth's crust. Hydronium ion (H_3O^+) hydration by water clusters in steam and low density supercritical water vapor "determines" the pH of such low density aqueous media at elevated temperatures, which in turn, affects the reactivity of water vapor, with particular reference to gas–solid interaction in the Earth's crust.

The last decade has seen a sharp increase in the study of large water clusters with up to 1000 H_2O molecules and 1–3 nanometer size ranges (Devlin et al. 2000. Buch et al. 2004). The drive to study these cluster systems stems from a desire to understand the composition and structure of cluster, droplet (and bubble) surfaces (Vácha et al. 2007, Buch et al. 2007) and the role such surfaces can play in vapor-liquid isotope exchange reactions, seawater spray and aerosol chemistry, and molecular speciation during bubble formation (boiling) and droplet nucleation in vapor. Studies of water clusters have also become relevant in the context of interpreting results of water droplet zeta-potential measurement and droplet titration experiments, as these indicate a propensity of some ions to concentrate at water cluster surfaces (Buch et al. 2007). For instance, a number of recent reports have demonstrated enhanced autoionization of water molecules at solution-gas interfaces resulting in acidic ($pH < 2$) water surfaces (Vácha et al. 2007). The enhanced surface propensity of the aqueous H_3O^+ ion has also been deduced from gas-phase IR-predissociation spectroscopic experiments with both Eigen- and Zundel-type proton water clusters present throughout the interfacial region of small water clusters (Headrick et al. 2005). A similar asymmetric surface solvation behavior has been reported for the halide ions Cl^-, Br^-, and I^- (Robert and Johnson 2003). Interestingly, halide–water clusters exhibit characteristic discontinuities in their solvation enthalpy and entropy profiles, a feature that is rationalized by invoking halide–water clusters with surface solvation motifs (Likholyot et al. 2005). In contrast, the smaller ion water clusters, $F^-(H_2O)_n$ and $OH^-(H_2O)_n$, form strong proton-acceptor bonds with water, and, in general, exhibit interior or near-surface solvation behavior as the cluster size evolves beyond $n \sim 15$ (Robert and Johnson 2003)

A large number of mass spectrometric, IR spectroscopic and theoretical studies have explored the molecular structure of protons and OH^- ions in water clusters (Hodges and Wales 2000; Chang et al. 2005; Headrick et al. 2005; Meot-Ner 2005; Douberly et al. 2010; and refs. therein), and these efforts have centered around the structure of the H_3O^+ and OH^- ions on the droplet surface and interior using two basic structural motifs: for the proton, the Eigen cation

($H_9O_4^+$) and the proton-sharing Zundel ion ($H_5O_2^+$), (Headrick et al. 2005) and, in the case of OH^-, a 4-water versus 6–7 water solvation shell configuration of the hydroxide ion near the surface and in the droplet interior (Robertson et al. 2003), respectively. One of the crucial aspects of water autoionization reactions in water nanodroplets is therefore the energetic gain as the H_3O^+ ion is transferred from the droplet interior to the surface, and the interior stabilization of the OH^- ion. In the case of the "pure" protonated water droplet, results from MD-based structure searches and DFT calculations of a model ($H_{97}O_{48}^+$) cluster (Vácha et al. 2007) suggest that an Eigen-like proton configuration in which the H_3O^+ ion occupies a droplet surface position is around 8–10 kcal/mol lower in energy than when the proton resides in the droplet interior. These results align with basin-hopping B3LYP calculation of medium sized proton–water clusters, $H_{43}O_{21}^+$ (Kozack and Jordan 1993) and $H_{19}O_9^+$ (Do and Besley 2012) that demonstrate a surface propensity for protons in water clusters.

Several interesting features emerge from these results. Water cluster (and droplet) pH is a surface phenomenon, in which the proton surface concentration increases around 200-fold relative to the bulk yielding a highly acidic water surface with pH values ranging from 1.8 to 4.2 (Vácha et al. 2007), and, up to ~30% of surface protons exist as protonated water dimers (i.e. the Zundel ion $H_5O_2^+$) with characteristic IR fingerprint bands in the 1055–1085 cm^{-1} spectral region (Headrick et al. 2005). The proton therefore prefers solvation at the surface of a water cluster or droplet and this behavior is rooted in the fact that the H_3O^+ and the $H_5O_2^+$ ions can establish 3 and 4 strong hydrogen bonds with neighboring water molecules. However, due to the small partial charges on the oxygen atoms, both ions are only weak hydrogen bond acceptors and thus poor network builders inside the water droplet/cluster. Interestingly, this surface propensity of H_3O^+ (and $H_5O_2^+$) has been observed for magic-number proton water clusters as in $H^+(H_2O)_{21}$ (Shin et al. 2004) and slab-like water surfaces (Jungwith and Tobias 2006), showing that the proton exhibits a strong preference for the air/water interface with important consequences for surface water acidity, in particular, at molecular depths of around 1 μm.

Similar studies carried out for solvation in the hydroxide–water cluster $H_{95}O_{48}^-$ show that the energy of the cluster with interior OH^- solvation is lower in energy by about 5 kcal/mol than the best surface configuration (Vácha et al. 2007). In other words, water autoionization and ion solvation at water-gas interfaces results in surface accommodation of the proton, while the hydroxide ion is nested close to the surface or in deeper subsurface sites. The situation for water clusters and droplets is probably somewhat different due to surface tension effects; Figure 6 shows the isolated H_3O^+, $H_5O_2^+$ and OH^- ions as they appear (in blue) in a 1.5–2 nm-sized water cluster/droplet containing 48 water molecules.

Molecular simulation results have been obtained for the solvation of the ion-pair H_3O^+ and OH^- as it would occur upon autoionization in a cluster containing 47 water molecules (Fig. 7 below). The most significant application of such H_3O^+/OH^- droplet solvation processes

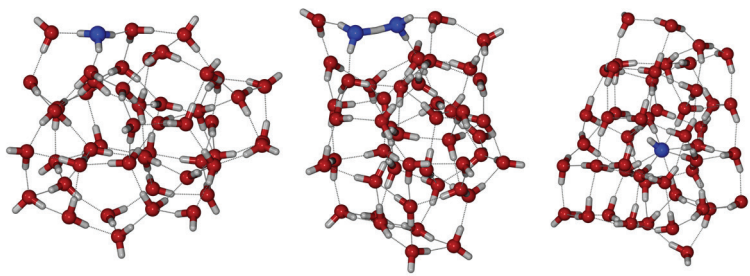

Figure 6. Global minima structures of $[H_{97}O_{48}]^+$ with Eigen and Zundel surface solvation motifs (**left** and **center**) and $[H_{95}O_{48}]^-$ (**right**) with a 7-fold coordinated interior hydroxide ion; cluster structures obtained using a swarm optimization algorithm coupled with TIP4P, and reoptimized at M06–2X/aVDZ level of theory.

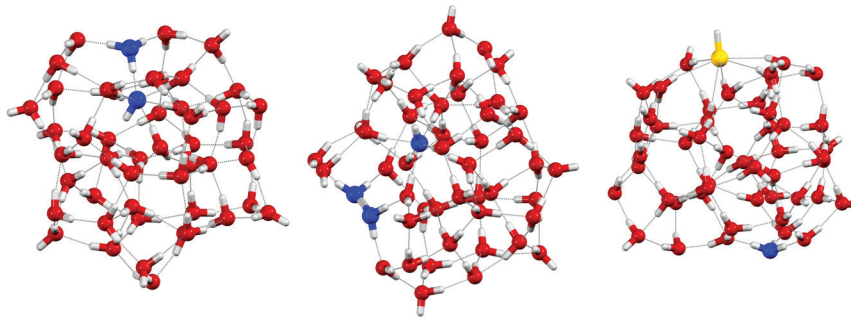

Figure 7. Global minima structures of proton–hydroxide and proton-bisulfide ion containing water clusters. Eigen-type $[H_3O]^+[OH]^-(H_2O)_{47}$ cluster with a surface proton and near-surface hydroxide ion pair **(left)**: $[H_5O_2]^+[OH]^-(H_2O)_{46}$ cluster containing a solvent-separated Zundel proton–hydroxide ion pair **(center)** and a proton-bisulfide water cluster $[H_3O]^+[SH]^-(H_2O)_{47}$ in which both ions are located on the opposite sides of the cluster surface **(right)**.

lies with H_2O autoionization reactions in/on aqueous nano-droplets and bubble surfaces during condensation and boiling processes, respectively, and are of importance in understanding surface charge distribution and nano-scale water autoionization trends (pK_w) in small water droplets; a more detailed discussion of water cluster ionization and size-effects on pK_w is provided further below. A summary of results obtained for the solvated H_3O^+/OH^- and $H_5O_2^+/OH^-$double ions is shown in Figure 7. For the Eigen-type cluster $[H_3O]^+[OH]^-(H_2O)_{47}$, the hydroxide ion is shifted outward to the droplet surface and ion pairs with the surface proton to yield a near-surface bound complex, as shown in Figure 7. For the Zundel-proton hydroxide ion pair, the hydroxide collapses back into the droplet center resembling a solvent separated ion pair; interestingly, a comparable surface solvation propensity has been reported for the larger halide ions, in particular, for bromide and iodide using empirical pair potentials (Jungwirth and Tobias 2002), quantum chemical calculations and spectroscopic measurements of mass-selected $Br^-(H_2O)_n$ and $I^-(H_2O)_n$ clusters (Ayotte et al. 1998; Lee and Kim 2001; Lee et al. 2002; Masamura 2003).

Finally, we note that mass spectrometric studies of protonated-water clusters by Yang et al. (1989) and Likholyot et al. (2007) demonstrated that the incremental solvation reaction from $H_3O^+(H_2O)_5$, $H_3O^+(H_2O)_6$ to $H_3O^+(H_2O)_7$, clusters with Zundel solvation motifs, are less favorable than solvation reactions involving neighboring smaller ($n<5$) and larger ($n>8$) clusters (see Fig. 8). As seen, the largest discontinuity in the stepwise solvation enthalpy and entropy occurs at around $n=5$–8, with two moderate discontinuities at $n=9$–11 and $n=20$–21. This first discontinuity and major endergonic shift in the stepwise proton solvation free is due to a large negative entropic contributions, and this feature is reflected in a dip in the solvation entropy profile at $n=6$ (−47.3 cal/mol/K; $T\Delta S$ = −14.1 kcal/mol) and $n=7$ (−52.1 cal/mol/K, $T\Delta S$= −15.5 kcal/mol); thus, these clusters are often referred to as anti-magic number clusters given their reduced stability. The second discontinuity at $n=20$–21 gives rise to a minor but noticeable exergonic shift in the free energy profile, and has been interpreted by invoking a surface solvated magic-number cluster with dodecahedral structure and enhanced stability (Wu et al. 2005).

Although mass spectrometric techniques are frequently employed for the measurement of ionic water clusters, tools for characterizing the nature of the proton–water and water hydrogen bonding environment, such as IRMPD in combination with mass spectrometry are relative new and are rapidly evolving techniques. Among these, the IR spectroscopic studies of Johnson and coworkers for $H_3O^+(H_2O)_{1–10}$ (Headrick et al. 2005), Miyazaki and coworkers for $H_3O^+(H_2O)_{3–26}$ (Miyazaki et al. 2004) stand out, as well as the recent IRMPD/MS studies of larger $H_3O^+(H_2O)_{19–49}$ clusters by Mizuse and Fujii (2013); the interested reader is also referred to a comprehensive review of recent *ab initio* work on the $H_3O^+(H_2O)_{4–27}$ cluster series given by Chang et al. (2007).

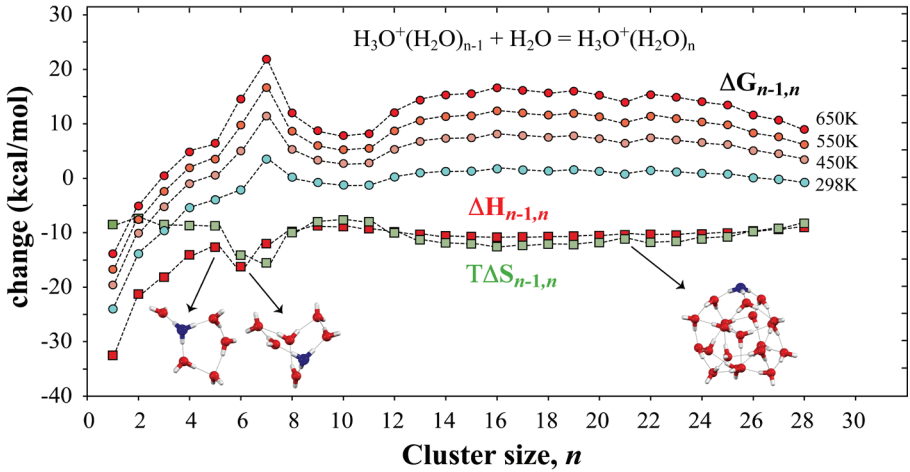

Figure 8. Incremental free energies (blue), enthalpy (red) and 298.15 entropy (green) profiles for the reaction $H_3O^+(H_2O)_n + H_2O = H_3O^+(H_2O)_{n+1}$ with $n = 1$–28; solvation free energies at 298 K (light blue) and temperature-dependent free energies at 50 K increments up to 650 K (dark red); all thermochemical data taken from NIST library.

From a geochemical point of view, gas-phase proton water interactions are the heart of understanding the concept of water vapor pH, as well as a wide range of related topics, such as water cluster/droplet autoionization processes, surface versus interior ionization of water clusters/droplets, and in particular, the pH-dependent speciation of metal complexes on proton-enriched cluster surfaces and proton-depleted interior regions; a particularly relevant application of the surface propensity of protons is the surface acidification of vapor-phase water clusters and droplets that form in high-temperature vapor along the liquid–vapor phase boundary. For instance, vapor condensation and evaporation processes are generally thought to occur instantaneously with little or no molecular preparation. In other words, the accepted view is that condensation and evaporation processes are best described using single-molecule and bulk solution thermodynamics, in combination with interfacial equilibria (Jungwirth and Tobias 2006). This approach, however, lacks crucial molecular-scale information into the vapor-phase clustering of water molecules. This is especially important at lower pressures, and in the vicinity of the liquid–vapor curve, where hydration reactions would be expected to generate a characteristic Boltzmann distribution of cluster sizes at each temperature and pressure. In the same way that liquid-like nanodroplets exits in the vapor above the bulk boiling temperature, it is conceivable that gas-phase bubbles form in the liquid–vapor transition region below the bulk boiling temperature, with characteristic temperature- and pressure-dependent bubble-size distributions.

The reduced sulfur species, HS^- and H_2S. The situation is quite different in the case of the proton-bisulfide water cluster. In this case, the solvation environment in the water droplet was modified such that the OH^- ion was replaced with HS^- and the cluster was equilibrated as in the initial simulation for the H_3O^+/OH^- droplet system. Figure 9 shows that the larger bisulfide ion forms weak acceptor hydrogen bonds surrounded by six water molecules and is nested on the cluster surface, while the proton prefers characteristic asymmetric surface solvation with three surface water molecules. In general, results presented in Figure 9 align well with results from previously reported *ab initio* calculations. For instance, Maeda et al. (2008) examined the smaller $[H_3O]^+[HS]^-(H_2O)_8$ and $[H_2S](H_2O)_9$ clusters using a combination of MP2 and B3LYP level of theory, and demonstrated that both H_3O^+ and HS^- are surface solvated ions and in equilibrium with neutral $[H_2S](H_2O)_9$, with the later forming a stable species in which

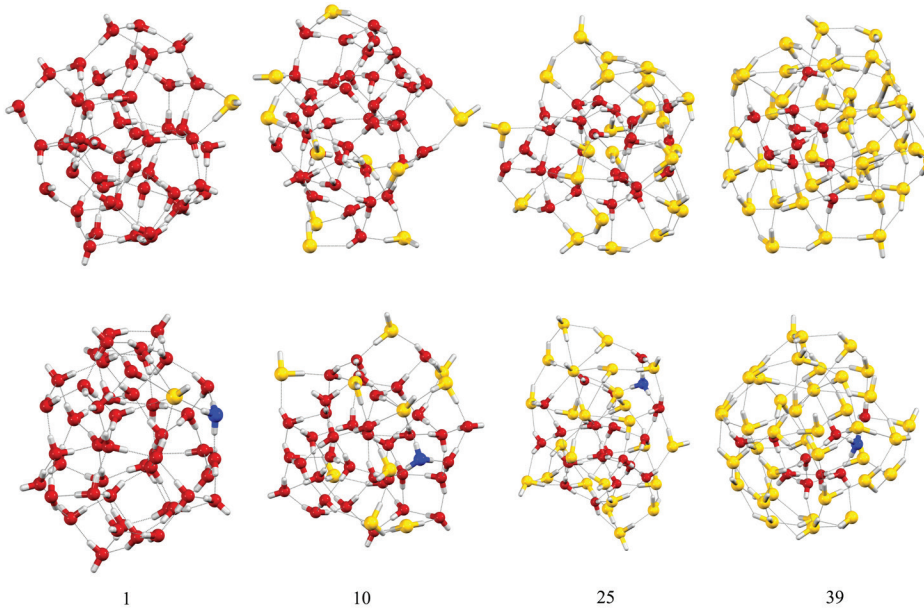

Figure 9. Global minima structures of neutral $(H_2S)_n(H_2O)_{49-n}$ **(upper row)** and ionic $(HS^-)(H_3O^+)(H_2S)_{n-1}(H_2O)_{48-n}$ **(bottom row)** clusters labeled according to the number of molecules of hydrogen sulfide (with $n = 1$, 10, 25 and 39) showing surface H_2S and interior H_2O domains; proton ion shown in blue.

the H_2S molecule is solvated on the surface of a $(H_2O)_9$ cluster. They also concluded that H_2S is surface-solvated onto water clusters at temperatures above 300 K, while fully solvated $(H_2S)(H_2O)_9$, i.e. clusters with interior H_2S, exist at lower temperatures. Smith et al. (1999) studied the structures and energetic properties of neutral $[H_2S](H_2O)_n$ clusters with $n = 4, 7$ and corresponding zwitterions $[HS^-][H_2O^+](H_2O)_3$ and $[HS^-][H_2O^+](H_2O)_6$ with MP2 and B3LYP level of theory, and found that the ionization energy ΔE (with ZPE correction) $[H_2S](H_2O)_4$ and $[H_2S](H_2O)_7$ to form the zwitterion clusters is around 8.8 and 1.9 kcal/mol, respectively. They attributed the enhanced stabilization of the $[HS^-][H_2O^+](H_2O)_6$ zwitterion versus that of $[HS^-][H_2O^+](H_2O)_4$ to hydrogen bonding effects within the second solvation shell in $[H_2S](H_2O)_7$ leading to transition state that is energetically close to the ion pair structure. Using MP2 theory, these authors also predicted free energies for the ionization processes $[H_2S](H_2O)_4 = [HS^-][H_2O^+](H_2O)_3$ and $[H_2S](H_2O)_7 = [HS^-][H_2O^+](H_2O)_6$ at 17.2 kcal/mol and 9.9 kcal/mol, respectively. Interestingly, the latter value is consistent with the reported first ionization energy for H_2S of 9.5 kcal/mol obtained for in aqueous solution (Suleimenov and Seward 1997).

Given the key role that water and H_2S/HS^- play in hydrothermal vapors, both as a reaction medium and as coordinating ligand, we have conducted a set of exploratory DFT calculation for the clusters $(H_2S)(H_2O)_{48}$, $(H_2S)_{10}(H_2O)_{39}$, $(H_2S)_{24}(H_2O)_{25}$ and $(H_2S)_{39}(H_2O)_{10}$, and their ionic forms, with the aim to highlight how changes in composition influence cluster mixing/unmixing and the surface propensity of H_2S and H_2O, but more importantly, to estimate composition-dependent changes of the H_2S ionization energy and how well these DFT prediction align with bulk values. As seen from Figure 9, water molecules are fully encapsulated into the cluster interior and capped by H_2S surface layers, with the former retaining water cluster-like configurations as in $(H_2S)_{39}(H_2O)_{10}$. This molecular immiscibility can be best understood qualitatively from a comparison of the SH···S binding energy in the H_2S dimer (Lemke 2017), which is significantly weaker than the OH···O hydrogen bond in the water dimer, by around 1.5 kcal/mol (Rocher-Casterline et al. 2011). At lower temperatures,

these clusters gain in thermodynamic stability through enthalpic contributions by increasing the number of hydrogen bonds. At higher temperatures, however, the gain in stability stems primarily from vibrational entropic effects leading to an unmixing of the hydrogen bonded network and a propensity of H_2S to migrate to the cluster surface.

The structure of the ion cluster $(HS^-)(H_3O^+)(H_2O)_{48}$ is strikingly similar to that of neutral $(H_2S)(H_2O)_{48}$, except that the former is a structure with a surface-solvated ion pair (HS^-–H_3O^+) and is around 6 kcal/mol higher in energy than neutral $(H_2S)(H_2O)_{48}$; the minimum energy structure for $(HS^-)(H_3O^+)(H_2S)_9(H_2O)_{38}$ contains a surface-solvated HS^--H_3O^+ ion pair and maintains a discontinuous surface shell of H_2S molecules that only partially covers the water core. Our DFT calculations show that the H_2S outer solvation shell evolves, with increasing number of hydrogen sulfide molecules, from a discontinuous monolayer at $n=10$, a monolayer at $n=25$, to a continuous bilayer with around 1 μm thickness at $n=39$. We did not observe any HS^-–H_3O^+ ion pairing in clusters with $n=25$ and $n=39$, instead, we find that the HS^- ions binds preferentially into the H_2S surface layers, whereas the proton resides solvated as an Eigen-ion in the central water-rich region of the cluster. Thus, the overall effect of increasing the hydrogen sulfide content in $(H_2S)_n(H_2O)_{49-n}$ from 2% ($n=1$) 20% ($n=10$), 50% ($n=25$) to 80% ($n=39$) is to induce a nano-scale phase separation with a water core and H_2S surface.

THE ION PRODUCT CONSTANT, K_W, OF STEAM

With the exception of studies on steam pH by Klots (1984), there have been only limited studies concerning the role of protons (and hydroxide ion) in high-temperature water vapor (Lemke and Seward 2008b, and refs therein). Tanger and Pitzer (1989) reported low-density H_2O ionization constants pK_w ($=-\log K_w$) in the temperature range from 298 to ~2000 K and these show, for instance, that pK_w values for vapor-water ionization at 1 bar shift by ~30 orders of magnitude to larger values when the temperature is shifted from 298 K to magmatic values of ~1200 K, in other words, heating aqueous vapors at constant pressure induces water ionization and favors the formation of gas-phase protons and hydroxide ions; similarly, water vapor ionization is enhanced by around 25 orders of magnitude when the pressure in increased at constant temperature (673 K) from 0.1–25 MPa Tanger and Pitzer (1989). Thus, ionized water clusters and nanodroplets are likely to play a central role in the vapor phase chemistry and reactivity in volcanic gas systems. As mentioned earlier, the thermodynamic properties of individual proton- and hydroxide–water clusters have been studied in detail both experimentally and using molecular simulation tools, however, only a few studies exist in which the combined proton–hydroxide water cluster system has been examined (Perlt et al. 2017).

A major gap in our understanding of gas-phase ionization of water stems from a lack of data on the ionization thermochemistry of water clusters, in particular the proton–hydroxide water system, the proton and hydroxide solvation structure, and the influence of cluster size on the water autoionization constant K_w. Likewise, there are no data available describing effects of temperature on water ionization energies in water clusters or even nanodroplets. With this knowledge gap in mind, we have explored how water clusters ionize and provide some preliminary data on the ionization constant K_w as a function of cluster size and temperature. Insight from our preliminary theoretical work is described below and includes a comparison against recently reported at values of pK_w obtained from MP2 and DFT proton–hydroxide water cluster calculations (Perlt et al. 2017). At the end of this section, we will briefly discuss the implications for the ionization of water vapor, and the consequences of proton and hydroxide ion partitioning into surface, near- surface and interior sites of water clusters.

A summary of the key thermodynamic properties for the gas-phase ionization of water, and the influence of water cluster size and thermal effects are given in Table 1. Clearly, the pK_w values listed below cannot be directly compared against bulk water ionization constants,

Table 1. M06–2X/aVDZ ionization energies and associated thermodynamic properties for water clusters as in $(H_2O)_n = H_3O^+–OH^-(H_2O)_{n-2}$ at 1 bar where the units for the ZPE-uncorrected ionization energy ΔE_e are in kcal/mol; values for the ionization free energy (ΔG) and enthalpy (ΔH) are given in kcal/mol and ΔS is given in cal/mol/K.

n,*n*–2	ΔE_e	$\Delta H_{298\,K}$	$\Delta S_{298\,K}$	$\Delta G_{298\,K}$	$pK_{w(298\,K)}$	$\Delta G_{500\,K}$	$pK_{w(500\,K)}$
10,8	7.7	6.2	–2.4	7.0	5.1	7.4	3.2
15,13	11.3	9.6	–2.6	10.3	7.6	10.9	4.8
20,18	11.6	9.9	–7.5	12.2	8.9	13.7	6.0
25,23	12.6	7.1	–0.5	7.3	5.4	7.4	3.2
30,28	10.7	8.4	–0.1	8.5	6.2	8.5	3.7
35,33	11.1	7.9	–2.6	8.7	6.4	9.2	4.0
40,38	17.8	13.6	1.3	13.2	9.7	13.0	5.7
45,43	10.7	7.1	–2.3	7.8	5.7	8.3	3.6
50,48	16.0	14.3	–6.0	16.1	11.8	17.4	7.6
55,53	30.8	27.6	–0.1	27.7	20.3	27.6	11.9
60,58	31.6	28.8	3.3	27.9	20.5	27.2	11.9
65,63	17.8	16.6	–3.7	17.7	13.0	18.5	8.1
70,68	29.5	27.7	0.3	27.6	20.3	27.5	12.1

nevertheless, a set of rigorous ionization energies derived from global minima proton–hydroxide water clusters have been derived and a comparison with recent *ab initio* results and trends obtained from gas-phase high-temperature experiments is given below. Interestingly, recent theoretical calculations of pK_w using clusters with up to 10 water molecules (Perlt et al. 2017) indicate that values of pK_w display a strong dependence on the choice of DFT method and cluster size range spanning values of pK_w from 12 (PBEO-D3) to 44 obtained with high level CCSD(T) theory. Water ionization energy values obtained at the M06–2X level of theory for small (n = 10–35) to medium size water clusters (n= 40–70) are given in Table 1. Figure 10 display a selection of the proton–hydroxide water cluster structures together with their neutral precursors that have been used to predict water cluster ionization energies and the size- and temperature-dependent trends in pK_w; Figure 11 shows the size- and temperature-dependent trends in pK_w for water clusters in the size range n = 10–70.

As seen Table 1, theoretically determined structures and vibrational analyses place our water cluster ionization enthalpies, ΔH, at ~6–9 kal/mol, which is significantly less than the corresponding ΔH_{K_w} bulk water value of 13.3 kcal/mol (Holzapfel 1969). The corresponding values for $T\Delta S$ (298 K) for clusters listed in Table 1 are less than ~2 kcal/mol and do not vary significantly as a function of cluster size indicating that the water network for n = 10–70 remains largely unchanged in terms of the basic hydrogen bonding network structure. $T\Delta S$ represent a minor (~5%) contribution towards the total ionization free energy. These reduced entropic contributions for the smaller cluster size ranges are somewhat surprising when we consider that there are large deviations between the structures of neutral and ionized water clusters. For instance, the neutral clusters $(H_2O)_{10}$ are mainly populated by stacked water pentamer rings and related isomers, whereas ionic species are predominantly cube-like as in $OH^-H_3O^+(H_2O)_8$ (see Fig. 10). It is also noteworthy that ionization energies for water clusters, beginning with n = 55, shift toward higher ionization energy values of ~23 kcal/mol at 298 K (~pK_w = 16) and decrease steadily with increasing temperature at equilibrium vapor pressures (i.e. "along" the

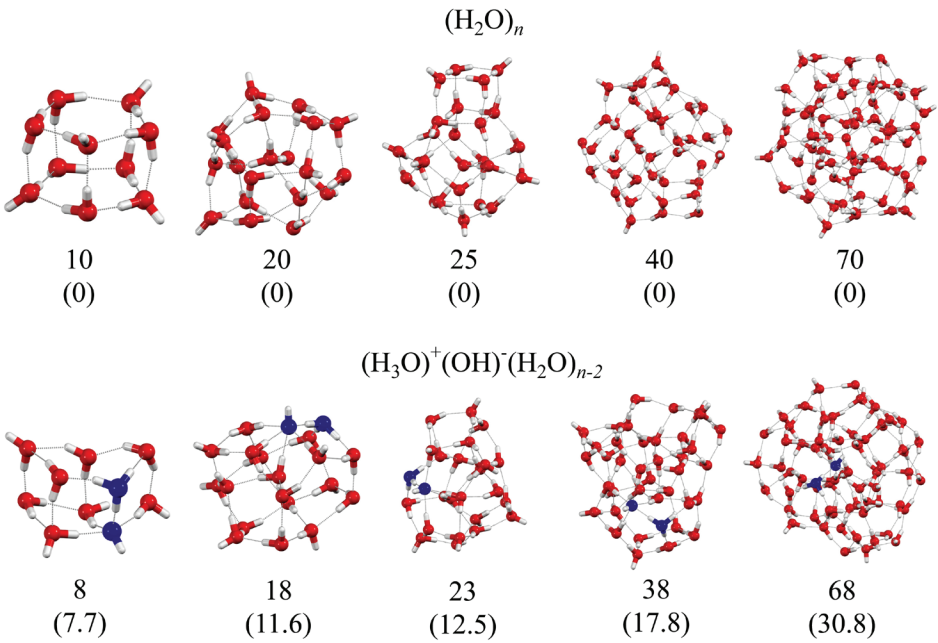

Figure 10. M06–2X/aVDZ geometries for neutral $(H_2O)_n$ and ionized water clusters $(H_3O)^+(OH)^-(H_2O)_{n-2}$ with n=10, 20, 25, 40 and 70; relative energies (kcal/mol) for neutral and ion clusters shown in parenthesis.

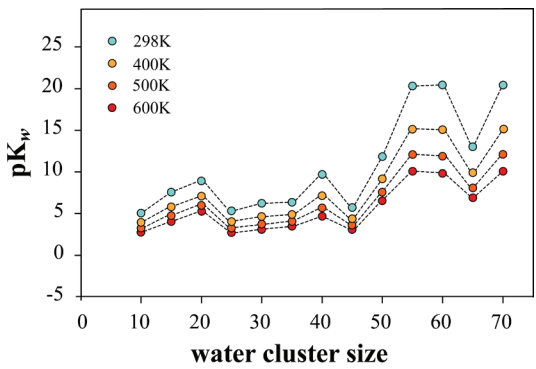

Figure 11. The dependence of the ionization constant pK_w for $(H_2O)_n = (H_3O)^+(OH)^-(H_2O)_{n-2}$ on water cluster size and temperature obtained M06–2X/aVDZ level optimizations and frequency calculations.

2-phase curve); for example, the pK_w value for the water cluster ionization reaction $(H_2O)_{25} = OH^-H_3O^+(H_2O)_{23}$ shifts from 5.4 (298 K), 4.0 (400 K), 3.2 (500 K) to 2.7 (600 K). These pK_w values are significantly different from the corresponding bulk solution values of liquid water at 298 K (14.0), 400 K (12.0) 500 K (11.2) 600 K (11.6). Thus, there is a significant vapor-phase enhancement of the ionization of water.

Perhaps the most intriguing finding from these survey calculations is that the majority of calculated water cluster ionization energies (ΔG) listed in Table 1 are significantly more favorable than the 19 kcal/mol (298 K) bulk solution value, the notable exception being water ionization energy values for larger clusters in the size range n>55. The second important feature observed for the proton–hydroxide water clusters is the propensity for both ions to partition to the water cluster surface, which clearly differs from proton and hydroxide surface

solvation processes that take place at air/liquid water interfaces (Jungwirth and Tobias 2006). For the air/liquid water interface, there is clear evidence, both from experiment and from *ab initio* calculations (Jungwirth and Tobias 2006, and references therein), that the hydronium ion prefers surface solvation, whereas hydroxide ions reside in the solution interior and exhibit a near-surface propensity at most (Vacha et al. 2007). Extending our current DFT simulation results to the aqueous vapor environment, we may therefore expect that water cluster (droplet) ionization reactions exhibit pronounced cluster-size dependencies leading to a characteristic size distribution of proton–hydroxide water clusters reflective of temperature and water monomer pressure. These theoretical results also indicate that for a given cluster-size, the proton and hydroxide ions will surface-solvate either as contact ion pairs ($n = 20$–55) or as solvent-separated ion pairs ($n > 70$), posing interesting questions about charge separation and surface versus interior solvation motifs in larger water clusters upon ionization.

SODIUM CHLORIDE IN STEAM/LOW DENSITY WATER VAPOR

Of particular interest in high-temperature, low-density aqueous systems (i.e. in steam and supercritical aqueous fluids having gas-like densities) is the well-known solubility of many inorganic compounds (Palmer et al. 2004) in such media. In natural volcanic gas and magmatic volatile systems, NaCl and other halogen compounds (e.g. HF, HCl, NH_4Cl, HBr) are ubiquitous and NaCl and HCl in particular, play an important role solid–gas reactions in low-pressure magmatic and volcanic gas environments. The vapor pressure of crystalline NaCl (melting point 800.7 °C; boiling point 1465 °C: CRC Handbook 2013) iv th[e] absence of water is low, varying from 4.9×10^{-8} bar at 500 °C but then rising to 3.8×10^{-4} bar at 790 °C, just below the NaCl melting point (Zimm and Mayer 1944; Ewing and Stern 1974; Dortmund Data Bank 2018). However, the concentration of NaCl is many orders of magnitude higher in steam or low density, supercritical water than in a "dry" system without water as demonstrated by various experimental studies (Martynova 1964; Styrikovich et al. 1966; Galobardes et al. 1981; Armellini and Tester 1993) and further summarized by Palmer et al. (2004). These earlier studies were motivated by a need to understand NaCl volatility/solubility in steam and salt transport in steam and related corrosion problems in power generation systems.

The solubility of NaCl in water vapor is a function of the density of the "steam" phase, temperature and pressure but reliable solubility data are sparse at low steam densities and the molecular details are not well known. However, some insight is provided by a number of computational studies (e.g. Pitzer 1983; Fernandez-Prini 1998; Suleimenov et al. 2006). It is well known that sodium and chloride ions are extensively ion paired in aqueous (liquid) electrolyte solutions at elevated temperatures up to 600 °C and moderate pressures up to 1000 bar (Quist and Marshall 1968). It has also generally been accepted that NaCl ion pairing defines molecular speciation in steam as well. In their thermodynamic study of NaCl in steam, Pitzer and Pabalan (1986) considered that NaCl–water clusters (their successive hydration model) were responsible for the observed solubilities. More recently, Suleimenov et al. (2006) employed CBS-QB3 level theory (Montgomery et al. 1999) to obtain gas-phase Gibbs energies (for optimized cluster geometries) of various NaCl–H_2O clusters as a function of temperature and pressure which together with thermodynamic data for halite and water, permitted the calculation of NaCl solubility in steam. Other ab initio studies pertaining NaCl–water clusters as well as metal complex–water clusters such as $AgCl(H_2O)_n$ (e.g. Godinho et al. 2006) have been carried out but are not relevant to high temperature water vapor. Figure 12 shows the solubility of NaCl in water vapor at 450 °C as a function of pressure (or density). With increasing pressure or water vapor density, higher order clusters (i.e. $NaCl(H_2O)_6$ and $NaCl(H_2O)_8$) predominate and account for NaCl solubility in steam at 450 °C at pressures greater than 100 bar. At pressures < 100 bar, the $NaCl(H_2O)_4$ cluster becomes significant. However, at lower pressures < 10 bar (at 450 °C) and at higher temperatures and low pressures (low steam densities), the assumption that ion pairing accounts for NaCl solubility ignores the possible role of charged (ionic) species.

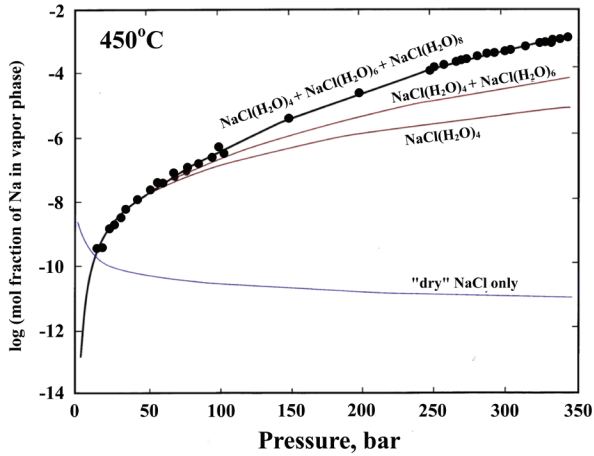

Figure 12. The solubility of NaCl in steam at 450 °C; experimentally measured values (full circles) are from Galobardes et al. (1981) and Rosenbauer and Bischoff (1987); the other curves refer to the calculated solubilities assuming the presence of $NaCl(H_2O)_n$ clusters with $n=4$, $n=4+6$ and $n=4+6+8$.

There are few experimental measurements pertaining to NaCl properties (e.g. solubility, conductivity; Lukashov et al. 1975) in low density/low pressure water vapor at elevated temperatures. However, some insight into ionic speciation and hydration in low density water vapor has come from mass spectrometric and quantum chemical (ab initio) studies (e.g. Kebarle 1977; Lau et al. 1982; Likholyot et al. 2005, 2007). Likholyot et al. (2007) studied proton–water clusters in water vapor pressures ≤ 0.3 mbar at temperatures up to 580 °C and identified proton water clusters with up to 8 waters at near ambient conditions with clusters containing only 2 waters appearing at temperatures >500 °C. In the case of chloride ion, clusters containing up to 8 waters were identified with a trend from exterior clusters (in which the Cl^- is bound to the surface of the water cluster) to classical interior clusters (Cl^- bound within the cluster) predominating as temperature increases to >500 °C (Likholyot et al. 2005). In addition, Pitzer (1983) has demonstrated (using mass spectrometrically derived thermodynamic data for Na^+ and Cl^- hydration together with NaCl solubility in steam and a general Born model approach) that there is an increase in ionic species in low density (e.g. 0.01–0.10 g/cm^3) steam containing NaCl with increasing temperature from 400 to 800 °C, although NaCl ion pairs still comprise a significant portion of the total dissolved salt. Our dilemma then, is that there are few experimental or theoretical studies of simple 1:1 and 2:1 salts in water solvent having gas-like density at high temperatures pertinent to magmatic and volcanic gas systems or to steam in lower temperature hydrothermal/geothermal systems and from which we can gain molecular insight into gas–solid equilibria and reactivity at these extreme conditions.

SOLVATION OF METALS IN WATER VAPOR

A major problem in gas-phase metal transport is the difficulty of assessing how metals and metal complexes bond to water clusters, and consequently the large uncertainty as to their abundance in water vapor. A brief review of the existing experimental data reported for gas phase metals shows that metals such as copper and gold are extremely partitioned into the vapor-phase upon boiling, however, there are only limited data available on the concentrations and structures of metal water clusters in different water vapor environments. Indeed, an understanding of the stability of metal-water clusters under typical hydrothermal conditions may provide a new perspective on metal ore formation from low-density aqueous fluids. Experimental studies of

hydrated metal clusters using electrospray ionization mass spectrometry and high temperature studies of metal halide complexes in water vapor, have established a conceptual bridge between metal ion cluster observed in high vacuum environments and the occurrence of a metal-charged vapors in nature (Schröder 2012). Subsequent experimental studies of solvated metal species have shown that the formation and stability of, for instance, gaseous gold (Mei et al. 2017) and copper complexes (Mei et al. 2018) is directly related to the size and structure of the solvation shell surrounding the metal core. One important conclusion from above mentioned studies is that a wide range of hydrated metal-water clusters would exist in the vapor phase at any given temperature and pressure, probably with one dominant global minimum configuration and a large number of coexisting local minima (for instance, the octa-hydrated gold cation has around 10 distinct minimum structures within a 1 kcal/mol energy range). There is a general consensus, from experimental and *ab initio* studies, that the gold(I) ion binds water with two H_2O molecules attached directly to the metal center. However, there is less of a consensus on the minimum energy structures adopted by Au(I) and chloride complexed Au(I) in larger water clusters or even nano-sized water droplets. The following section of this review will therefore give an account of the current understanding of gold solvation in water clusters, without a ligand and in the presence of a halide ion such as Cl^-.

Gold in water vapor and the cluster solvation of Au⁺. Several laboratories have reported mass spectrometric and vibrational spectra of charged gold–water clusters in an attempt to characterize the water network surrounding the gold atom. For instance, for the Au(I)–water system, Li et al. (2012) reported results from IRMPD spectroscopic studies of mass-selected $Au^+(H_2O)_n$ clusters with $n = 1–8$, showing that Au^+ retains two water molecules into its primary solvation shell forming a linear O–Au^+–O configuration. Subsequent water molecules attach to the H_2O–Au^+–OH_2 core forming the second solvation shell, which is complete at $n = 6$. The structure of the $Au^+(H_2O)_n$ cluster system was also described in detail using *ab initio* molecular dynamics simulations (Camellone and Marx 2012), MP2 and CCSD(T) level of theory calculations with up to six water molecules (Lee et al. 2005a,b) and DFT calculations at the PBE99 level of theory for larger $Au^+(H_2O)_n$ clusters with up to 10 water molecules (Reveles et al. 2007). Interestingly, results from the above simulations and those obtained from mass spectrometric studies of $Au^+(H_2O)_n$ (Magnera et al. 1989; Poisson et al. 2002) indicate that the second water solvation energy is larger (by around 5–6 kcal/mol) than the first solvation energy, a feature rooted in electronic and hybridization effects in Au^+–water clusters. In brief, the first two water molecules bind strongly to Au^+ at around ~40 and 45 kcal/mol, followed by a decrease in the binding energy from 23 to 16 kcal/mol for solvation by 3–6 H_2O molecules, and remain constant at condensation level values of ~10 kcal/mol for $n = 7–10$; the role of charge transfer in $Au^+(H_2O)_n$ clusters has been examined in detail by Lee et al. (2005), who described various contributions from 6s- and 5d-orbital hybridizations to the overall stability of mono-cationic $Au^+(H_2O)$. It is also noteworthy to briefly comment on how the water solvation shell contributes to the overall structure and stability of polynuclear gold clusters. A brief review of recent mass spectrometric and molecular simulation results for $[Au_m]^+(H_2O)_n$ is given below. One interesting aspect of water solvated poly nuclear gold clusters is a potential connection between the stability of a polynuclear gold cluster and the emergence of nano-sized gold particles in water vapor, as well as the influence of water desorption processes, at higher temperatures, on the onset of gold nucleation and precipitation in the gas-phase. For instance, gas phase microsolvated gold clusters would likely undergo a two-step water desorption process in which more loosely bound 2nd shell water molecules are released from the solvated core, followed by desolvation of more strongly bound water molecules that are in direct contact with Au atoms. For example, structures and water desorption energetics in $[Au_m]^+(H_2O)_n$ have been probed using TOF mass spectrometry and complimented with DFT and MP2 calculations (Nagata et al. 2017). Thermal effects were examined by observing changes in TOF mass spectra in the temperature range 300–1000 K, including shifts in the intensity and

distribution of hydrated gold cluster. In brief, these results showed that $[Au_m]^+(H_2O)_n$clusters incrementally release water molecules upon heating with characteristic intensity distributions (m/z $m\times197+n\times18$ a.u.). For example, for pentanuclear $[Au_5]^+(H_2O)_n$, desolvation is complete at 600 K, whereas smaller hydrates of $[Au_5]^+(H_2O)_n$ exhibit characteristic intensity maxima at 350 K ($n=4$), 420 K ($n=3$), 480 K ($n=2$) and 540 K ($n=1$). In other words, smaller solvation shells remain stable at elevated temperature and conversely, lower temperatures favor larger solvation environments. Interestingly, water dissociation energies for $[Au_2]^+(H_2O)_n$ incrementally increase with decreasing water shell cluster size ($n=4$–1), whereas water binding energies in the mono-solvated clusters $[Au_m]^+(H_2O)$ decrease with increasing gold cluster size ($m=2$–8). In the case of octa-nuclear gold, water binding energies shift form 14 kcal/mol ($n=1$), 9 kcal/mol ($n=2$), 8 kcal/mol ($n=3$) to 6 kcal/mol ($n=4$), and these size-dependent trends in water binding energies can be directly traced to the size of $[Au_m]^+$ core, and shifts in charge density of the ion core; a related study also reported MP2 and DFT level water binding energies for tri-nuclear $[Au_3]^+(H_2O)$, (13.4 kcal/mol) Ag-doped $[Ag_2Au]^+(H_2O)$ (10.8 kcal/mol) and $[Ag_3]^+(H_2O)$ (11.3 kcal/mol) (Fleischer et al. 2013).

From the above experimental and theoretical studies, it evolves that poly nuclear gold clusters, such as $[Au_5]^+(H_2O)_n$ and larger $[Au_m]^+(H_2O)_n$ species exist over a wide temperature range much like pure water clusters. Important yet unexplored aspects of poly nuclear Au cluster are whether the higher water partial pressures (and those of other volatiles) in natural hydrothermal systems would give rise to an expanded solvation shell, contributing towards a fully dissolved gas-phase gold cluster, and more importantly, how gold cluster abundances would balance, in response to changes in temperature and the significantly higher water vapor pressures in gas-like ore fluids compared against typical UHV conditions used in mass spectrometric studies. A final point of interest related to the transport of Au in low-density ore fluids, is the propensity of Au^+ ions, Au complexes and larger gold clusters to partition to water cluster (and nanodroplet) surfaces and/or interiors. In fact, the propensity of metals to surface-solvate or reside in the interior of a water cluster or droplet would have important consequences for metal complexation/clustering processes and the fractionation of isotopes given the fundamentally different thermodynamic properties of surface and bulk hydrated metal species. These themes have been discussed in detail for smaller ions, with reference to IR spectroscopy and quantum chemical calculations and it is now well known that the hydrated proton resides at the vapor/solution interface, giving rise to an acidic cluster surface, whereas the hydroxide ion partitions into the cluster interior resulting in an alkaline near-surface layer and a neutral pH in the deeper bulk region (Jungwirth and Tobias 2006). The surface, near-surface or bulk propensity of metal ions, complexes or clusters in water clusters and droplets remains unresolved at present, however this issue can be addressed in future using IR spectroscopy, mass spectrometry and a combination of molecular simulation tools.

Solvation of the AuCl complex in water vapor. Following our discussion on the structure and energetic properties of solvated gold ions and clusters, it is meaningful to provide a brief review of the gas-phase stability of halide-complexed gold species, particularly because, halide ions represent a core class of ligands that bind strongly to gold ions and occur ubiquitously in ore vapor environments. Complexation of gold with halide ions, but also other ligands, such as H_2S/HS^-, is a central topic in hydrothermal geochemistry, and its consequences for the mobility of Au have been discussed in detail, both for the bulk solution environment, and for ore vapors (Stefansson and Seward 2003; Seward et al. 2014; Hurtig and Williams-Jones 2014, Lemke 2014b). However, unlike for the ligand-free case, Au complexation with halide ions gives rise to a fundamentally different solvation environment around the halogen (in part due to weak X^-–H interactions) and also induces a restructuring of the solvation shell near the gold atom. The solvation of AuCl in water vapor is an important topic for geochemists, however, there are still knowledge gaps regarding the speciation of mono- and poly nuclear gold in small water clusters and even more so for more complex mixed solvent systems.

The AuCl complex is a geochemically important species with an affinity to partition into aqueous vapors (Archibald et al. 2001; Hurtig and Williams-Jones 2014), however, these thermodynamic studies provide no direct insight into the solvation shell structure and stability of $AuCl(H_2O)_n$ in water vapor. There are to our knowledge no theoretical or experimental data in the literature for the structure and vapor phase stability of microsolvated $AuCl(H_2O)_n$, either as a function solvation shell size or temperature. From *ab initio* calculations, we now know that the global minimum structure of $AuCl(H_2O)_n$ is a near-linear complex, with the chloride ion and water molecule occupying terminal positions; for smaller solvation numbers (n), water molecules attach onto the water terminus given the higher water–water binding energy versus the reduced binding energy of the chloride water cluster system. As noted in the work of Reveles et al. (2007), the primary solvation shell of monovalent gold typically contains two water molecules. We have expanded on this work, and list results from a set of preliminary DFT computations at the M06/aVDZ level of theory for $AuCl(H_2O)_n$ clusters with primary and secondary solvation shells, and provide detail of the structures, i.e. global minima configurations, as well as trends for the incremental binding energies; Figures 13 and 14 show the global and local minima of $AuCl(H_2O)_n$ with up to 10 water molecules, and a van't Hoff plot for the stepwise solvation of AuCl with up to 9 water molecules; corresponding water binding enthalpies, free energies and equilibrium constants for solvated AuCl at 298 K and elevated temperatures are listed in Table 2.

As seen in Figure 13, AuCl with an expanded water solvation shell (n = 5–10) prefers exterior solvation on a water cluster surface, similarly as in the case of the larger halides (Likholyot et al. 2005). This surface solvation feature is highlighted in Figure 13, which shows the mono-solvated complex $AuCl(H_2O)$ bound onto a water tetramer ring for n = 5, a book-like water hexamer for n = 7 and in the case of $AuCl(H_2O)_{10}$, the $AuCl(H_2O)$ complex occupies the edge-sites of a stacked water decamer. Table 2 also shows that the entropic contribution to the solvation free energy is approximately constant at condensation entropy values for n = 2–9 (or equivalent to a ~9–11 kcal/mol $T\Delta S$ contribution at 298 K).

We have also carried out supplementary calculations to determine the relative strengths of interactions between AuCl, H_2O, NH_3 and H_2S, in other words, the affinity of these volatiles to bind to Au and their capacity to form an interconnected network around the AuCl core. For example, we found that the CCSD(T)/aVDZ binding energies in $AuCl(H_2O)$, $AuCl(H_2S)$ and $AuCl(NH_3)$ shift from –25.1, –40.3 to –48.9 kcal/mol, indicating a strong affinity of AuCl for solvation with

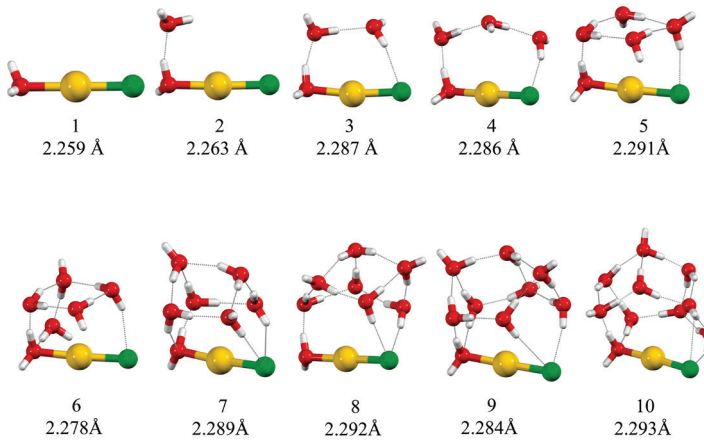

Figure 13. M06/aVDZ equilibrium geometries for $AuCl(H_2O)_{1–10}$ with Au–Cl distances given below each cluster; global minima obtained from swarm-based structure searches using TIP4P water Au–Cl force field parameters.

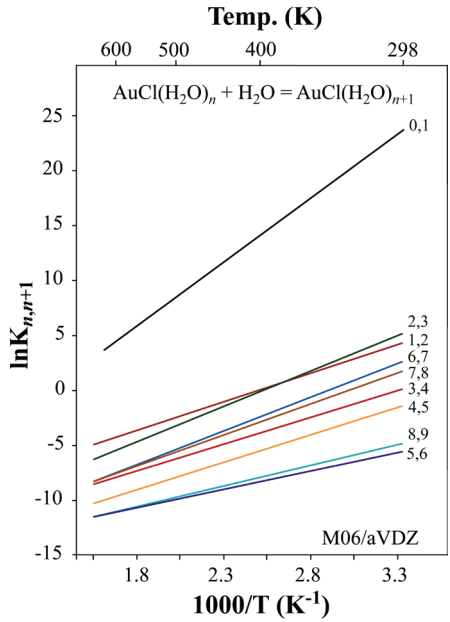

Figure 14. Van't Hoff plot for the incremental solvation of AuCl with first water listed as 0,1; attachment of additional H_2O molecules up to solvation step 8,9 shown as colored lines; the slope of the linear fits provide values of –ΔH which yield enthalpies for each successive solvation of $AuCl(H_2O)_n$ with $n = 0–9$.

Table 2. Incremental solvation energies of AuCl at the M06/aVDZ level of theory at 298 and 500 K at 1 bar, where the units for ΔE_e are in kcal/mol; ΔG, ΔH are kcal/mol and for ΔS, cal/mol/K.

$n, n+1$	ΔE_e	$\Delta H_{298\,K}$	$\Delta S_{298\,K}$	$\Delta G_{298\,K}$	$\ln K_{298\,K}$	$\Delta G_{500\,K}$	$\ln K_{500\,K}$
0,1	–24.5	–23.1	–29.9	–14.2	23.9	–8.1	8.2
1,2	–11.9	–10.3	–26.1	–2.5	4.3	2.8	–2.8
2,3	–14.3	–12.8	–32.7	–3.1	5.2	3.6	–3.6
3,4	–11.2	–9.7	–32.3	–0.1	0.1	6.5	–6.5
4,5	–11.7	–9.9	–36.2	0.9	–1.5	8.2	–8.2
5,6	–8.0	–6.6	–33.2	3.3	–5.6	10.0	–10.1
6,7	–14.4	–12.3	–36.1	–1.5	2.6	5.7	–5.8
7,8	–13.1	–11.2	–34.2	–1.0	1.7	5.9	–5.9
8,9	–8.9	–7.5	–34.8	2.9	–4.9	9.9	–10.0

the ammonia molecule; interestingly, the $AuCl(NH_3)$ binding energy is nearly double that of $AuCl(H_2O)$, and therefore solvation of AuCl is significantly more favorable than the formation of the corresponding hydrogen sulphide or even H_2O-bearing complex, with the only caveat that hydrogen-bond NH_3 networks are less stable than those formed by water. Finally, a wide range of hybridization and electronic effects will influence the magnitude and trends in the sequential solvation energies of AuCl, and these concepts will be of importance in understanding the solvation behavior of polynuclear gold chloride cluster in water vapor both with and without NH_3 and H_2S.

EPILOGUE

In this chapter, we have presented new data on the molecular structure of steam and water vapor and discussed various aspects of evolving cluster geometry and size as a function of temperature. We have then considered proton solvation in water vapor and shown that the hydronium ion occupies a surface coordinated position on water clusters which leads to an "acidic" nano-layer overlying a given molecular water cluster. New data on the ion-product constant of water vapor as a function of cluster size and temperature are also presented and this further encourages consideration of the molecular framework with which to consider the pH of water vapor at high temperatures. We note, for example, the values (Table 1) of pK_w(500 K) ranging from 3.2 to 6.0 for water cluster sizes (n = 10–45) in comparison to the liquid water value of pK_w(500 K) = 11.2.

The solvation of solute species in/on water clusters has also been considered by investigating the solvation of reduced sulfur (H_2S and HS^-) and a transition metal ion and complex (Au^+ and AuCl). H_2S was shown to prefer a surface hydration environment on water clusters resulting in a nano-scale phase separation comprising the water cluster core and an H_2S surface. Similarly, the simple AuCl complex is surface solvated on water clusters in water vapor. These and other observations discussed in our chapter emphasize the labile nature of high temperature water vapor with cluster surface enhanced availability of solute species, including charged species (e.g. protons). The much diminished pK_w of low density water solvent at high temperatures as well as the surface enhanced acidity of gas phase water clusters will also have fundamental implications for hydrolytic reactions and metal complex stability in water vapor. Of particular interest as well is the solvation of SO_2 by molecular water clusters in water vapor under conditions relevant to gas–solid (e.g. SO_2–feldspar) sulfidation reactions in high temperature porphyry and skarn deposits which give rise to ubiquitous anhydrite and the precipitation of sulfide minerals (Henley et al. 2017).

Over the past decade, there has been an accelerated progress in the field of gas phase physical chemistry, and in particular, researchers have made considerable advances in the field of cluster mass spectrometry and infrared spectroscopy. These advances have also been catalyzed by faster and more accurate *ab initio* tools and an improved capability to now study clusters one molecule at a time up to nanometer size ranges. Nevertheless, the study of neutral and ionic clusters in low-density water solvent under conditions relevant to the Earth's crust still remains a largely unexplored field of research.

ACKNOWLEDGMENTS

This work was supported by HK General Research Fund No. HKU 17302714. Computing time for this study was provided to K.H.L. by the HKU High Performance Computing (HPC) and Grid Computing Center.

REFERENCES

Archibald SM, Migdisov AA, Williams-Jones AE (2001) The stability of Au-chloride complexes in water vapor at elevated temperatures and pressures. Geochim Cosmochim Acta 65:4413–4423

Armellini FJ, Tester JW (1993) Solubility of sodium chloride and sulfate in sub- and supercritical water vapor from 450–550°. Fluid Phase Equil 84:123–142

Ayotte P, Bailey CG, Weddle GH Johnson MA (1998) Vibrational spectroscopy of small $Br^-(H_2O)_n$ and $I^-(H_2O)_n$ clusters: infrared characterization of the ionic hydrogen bond. J Phys Chem A 102:3067–3071

Barone V (2004) Vibrational zero-point energies and thermodynamic functions beyond the harmonic approximation. J Chem Phys 120:3059–3065

Braly LB, Liu K, Brown MG, Keutsch RS, Fellers RS, Saykally RJ (2000a) Terahertz laser spectroscopy of the water dimer intermolecular vibrations. II $(H_2O)_2$ J Chem Phys 112:10314–10326

Braly LB, Cruzan JD, Liu K, Fellers RS, Saykally RJ (2000b) Terahertz laser spectroscopy of the water dimer intermolecular vibrations. I $(D_2O)_2$ J Chem Phys 112:10293–102313
Buch V, Sigurd B, Devlin JP, Buck U, Kazimirski JK (2004) Solid water clusters in the size range of tens–thousands of H_2O: a combined computational/spectroscopic outlook. Int Rev Phys Chem 23:375–433
Buch V, Milet A, Vácha R, Jungwirth P, Devlin JP (2007) Water surface is acidic. Proc Nat Acad Sci 104:7342–7347
Buck U, Huisken F (2000) Infrared spectroscopy of size-selected water and methanol clusters. Chem Rev 100:3863–3890
Buck U, Ettischer I, Melzer M, Buch V, Sadlej J (1998) Structure and spectra of three-dimensional $(H_2O)_n$ clusters, n=8, 9, 10. Phys Rev Lett 80:2578
Buck U, Huisken F (2000) Infrared spectroscopy of size-selected water and methanol clusters. Chem Rev 100:3863–3890
Camellone MF, Marx D (2012) Solvation of Au^+ versus Au^0 in aqueous solution: electronic structure governs solvation shell patterns. Phys Chem Chem Phys 14:937–944
Casey WH, Rustad JR (2007) Reaction dynamics, molecular clusters, and aqueous geochemistry. Ann Rev Earth Planet Sci 35:21–46
Casey WH, Swaddle TW (2003) Why small? The use of small inorganic clusters to understand mineral surface and dissolution reactions in geochemistry. Rev Geophys 41:1008
Chang HC, Wu CC, Kuo JL (2005) Recent advances in understanding the structures of medium-sized protonated water clusters. Int Rev Phy Chem 24:553–78
CRC Handbook of Chemistry and Physics (2013) (WM Haynes, editor), 94th Edition. CRC Press LLC, Boca Raton FL, USA, 4–89
Dortmund Data Bank (DDBST GmbH) (2018)(www.ddbst.com/en/EED/PCP/VAP/ C4911.php)
Cruzan JD, Braly LB, Liu K, Brown MG, Loeser JG, Saykally RJ (1996) Quantifying hydrogen bond cooperativity in water: VRT spectroscopy of the water tetramer. Science 271:59–62
Curtiss LA, Blander M (1988) Thermodynamic properties of gas-phase hydrogen-bonded complexes. Chem Rev 88:827–841
Curtiss LA, Frurip DJ, Blander M (1979) Studies of molecular association in H_2O and D_2O vapors by measurement of thermal conductivity. J Chem Phys 71:2703–2711
Devlin JP, Joyce C, Buch V (2000) Infrared spectra and structures of large water clusters. J Phys Chem A 104:1974–1977
Do H, Besley NA (2012) Structural optimization of molecular clusters with density functional theory combined with basin hopping. J Chem Phys 137:134106
Douberly GE, Walters RS, Cui J, Jordan KD, Duncan MA (2010) Infrared spectroscopy of small protonated water clusters $H^+(H_2O)_n$ (n=2–5): isomers, argon tagging, and deuteration. J Phys Chem A 114:4570–4579
Ewing CT Stern KH (1974) Equilibrium vaporization rates and vapor pressures of solid and liquid sodium chloride, potassium chloride, potassium bromide, cesium iodide and lithium fluoride. J Phys Chem 78:1998–2005
Fernandez-Prini R (1998) Ionic aggregates in steam. 2. Standard chemical potentials. J Phys Chem 102;257–262
Feyereisen MW, Feller D, Dixon DA (1996) Hydrogen bond energy of the water dimer. J Phy Chem 100:2993–2997
Fleischer I, Popolan DM, Krstić M, Bonačić-Koutecký V and Bernhardt TM (2013) Composition dependent selectivity in the coadsorption of H_2O and CO on pure and binary silver–gold clusters. Chem Phys Lett 565:74–79
Galobardes JF, van Hare DR Rogers LB (1981) Solubility of sodium chloride in dry steam. J Chem Eng Data 26:363–366
Godinho SSMC, Cabral do Couto P, Costa Cabral BJ (2006) Photochemistry of AgCl–water clusters: Comparison with Cl^-–water clusters. Chem Phys Lett 419:340–345
Gregory JK, Clary DC, Liu K, Brown MG, Saykally RJ (1997) The water dipole moment in water clusters. Science 275:814–817
Grimme S (2006a) Semiempirical GGA-type density functional constructed with a long-range dispersion correction. J Comp Chem 27:1787–1799
Grimme S (2006b) Semiempirical hybrid density functional with perturbative second-order correlation. J Chem Phys 124:034108
Grimme S, Ehrlich S, Goerigk L (2011) Effect of the damping function in dispersion corrected density functional theory. J Comp Chem 32:1456–1465
Guimarães FF, Belchior JC, Johnston RL, Roberts C (2002) Global optimization analysis of water clusters $(H_2O)_n$ ($11 \leqslant n \leqslant 13$) through a genetic evolutionary approach. J Chem Phys 116:8327–8333
Guo X, Duursma M, Al-Khalili A, McDonnell LA, Heeren RM (2004) Design and performance of a new FT-ICR cell operating at a temperature range of 77–438 K Int J Mass Spectr 231:37–45
Headrick JM, Diken EG, Walters RS, Hammer NI, Christie RA, Cui J, Myshakin EM, Duncan MA, Johnson MA, Jordan KD (2005) Spectral signatures of hydrated proton vibrations in water clusters. Science 308:1765–1769
Henley RW, Seward TM (2018) Gas–solid reactions in arc volcanoes: Ancient and modern. Rev Mineral Geochem 84:309–349
Henley RW, Brink FJ, King PL, Leys C, Ganguly J, Mernagh T, Middleton J, Renggli CJ, Sieber M, Troitzsch U, Turner M (2017) High temperature gas–solid reactions in calc-silicate Cu-Au skarn formation; Ertsberg, Papua Province, Indonesia. Contrib Mineral Petrol 7211–7212
Hodges MP, Wales DJ (2000) Global minima of protonated water clusters. Chem Phys Lett 324:279–288
Holzapfel WB (1969) Effect of pressure and temperature on the conductivity and ionic dissociation of water up to 100 kbar and 1000°C J Chem Phys 50:4424–4428

Howard C, Gray JL, Hardwick AJ, Nguyen LT, Tschumper GS (2014) Getting down to the fundamentals of hydrogen bonding: anharmonic vibrational frequencies of $(HF)_2$ and $(H_2O)_2$ from ab initio electronic structure computations. J Chem Theory Comp 10:5426–5435

Huisken F, Kaloudis M, Kulcke A (1996) Infrared spectroscopy of small size-selected water clusters. J Chem Phys 104:17–25

Huisken F, Mohammad-Pooran S, Werhahn O (1998) Vibrational spectroscopy of single methanol molecules attached to liquid water clusters. Chem Phys 239:11–22

Hurtig NC, Williams-Jones AE (2014) An experimental study of the transport of gold through hydration of AuCl in aqueous vapour and vapour-like fluids. Geochim Cosmochim Acta 127:305–325

Johnston JC, Molinero V (2012) Crystallization, melting, and structure of water nanoparticles at atmospherically relevant temperatures. J Am Chem Soc 134:6650–6659

Jungwirth P, Tobias DJ (2002) Ions at the air/water interface. J Phys Chem B 106:6361–6373

Jungwirth P, Tobias DJ (2006) Specific ion effects at the air/water interface. Chem Rev 106:1259–1281

Kebarle P (1977) Ion thermochemistry and solvation from gas phase ion equilibria. Ann Rev Phys Chem 28:445–476

Keutsch FN, Saykally RJ (2001) Water clusters: untangling the mysteries of the liquid, one molecule at a time. Proc Nat Acad Sci 98:10533–10540

Klots CE (1984) The pH of steam. J Phys Chem 88:4407–4410

Kozack RE Jordan PC (1993) Structure of $H^+(H_2O)_n$ clusters near the magic number $n=21$. J Chem Phys 99:2978–2984

Lau YK, Ikuta S, Kebarle P (1982) Thermodynamics and kinetics of the gas-phase reactions—$H_3O^+(H_2O)_{n-1} + H_2O = H_3O^+(H_2O)_n$. J Am Chem Soc 104:1462–1469

Lemke KH (2014a) Structures and thermodynamic properties of $(C_2H_6)_n$ ($n=2$–8) by M06–2X and DFT-D theory: Implications for Titan's atmospheric chemistry. Chem Phys Lett 601:194–199

Lemke KH (2014b) Gold chloride clusters with Au (III) and Au (I) probed by FT-ICR mass spectrometry and MP2 theory. Phys Chem Chem Phys 16:7813–7822

Lemke KH (2017) Structure and binding energy of the H_2S dimer at the CCSD (T) complete basis set limit. J Chem Phys 146:234301

Lemke KH, Seward TM (2008a) Ab initio investigation of the structure, stability, and atmospheric distribution of molecular clusters containing H_2O, CO_2, and N_2O. J Geophys Res Atmos16:113

Lemke KH, Seward TM (2008b) Solvation processes in steam: Ab initio calculations of ion–solvent structures and clustering equilibria. Geochim Cosmochim Acta 72:3293–3310

Lemke KH, Seward TM (2013) Thermodynamic properties of carbon dioxide clusters by M06–2X and dispersion-corrected B2PLYP-D theory. Chem Phys Lett 573:19–23

Lee HM, Kim KS (2001) Structures and spectra of iodide–water clusters $I^-(H_2O)_{n=1-6}$: An ab initio study. J Chem Phys 114:4461–4471

Lee HM, Kim D, Kim KS (2002) Structures, spectra, and electronic properties of halide-water pentamers and hexamers, $X^-(H_2O)_{5,6}$ (X= F, Cl, Br, I): Ab initio study. J Chem Phys 116:5509–5520

Lee HM, Diefenbach M, Suh SB, Tarakeshwar P, Kim KS (2005a) Why the hydration energy of Au^+ is larger for the second water molecule than the first one: Skewed orbitals overlap. J Chem Phys 123:074328

Lee HM, Min SK, Lee EC, Min JH, Odde S, Kim KS (2005b) Hydrated copper and gold monovalent cations: Ab initio study. J Chem Phys 122:064314

Likholyot A, Hovey JK, Seward TM (2005) Experimental and theoretical study of hydration of halide ions. Geochim Cosmochim Acta 69:2949–2958

Likholyot A, Lemke KH, Hovey JK, Seward TM (2007) Mass spectrometric and quantum chemical determination of proton water clustering equilibria. Geochim Cosmochim Acta 71:2436–2447

Li Y, Wang G, Wang C, Zhou M (2012) Coordination and solvation of the Au^+ cation: infrared photodissociation spectroscopy of mass-selected $Au(H_2O)_n^+$ ($n=1$–8) complexes. J Phys Chem A 116:10793–10801

Liu K, Cruzan JD, Saykally RJ (1996a) Water clusters. Science 271:929–933

Liu K, Brown MG, Cruzan JD, Saykally RJ (1996b) Vibration-rotation tunneling spectra of the water pentamer: Structure and dynamics. Science 271:62–64

Liu K, Brown MG, Carter C, Saykally RJ, Gregory JK, Clary DC (1996c) Characterization of a cage form of the water hexamer. Nature 381:501

Lukashov YuM, Komissarov KB, Golubev BP, Smirnov SN, Svistunov EP (1975) Electrolytic properties of mono-monovalent electrolytes at high parameters of state. Teploenergetika 12:78–81

Lv ZL, Xu K, Cheng Y, Chen XR and Cai LC (2014) Ab initio investigation of the lower energy candidate structures for $(H_2O)_5^+$ water cluster. J Chem Phys 141:054309

Maeda S, Ohno K (2007) Structures of water octamers $(H_2O)_8$: Exploration on ab initio potential energy surfaces by the scaled hypersphere search method. J Phys Chem A 111:4527–4534

Maeda S, Ohno K (2008) Microsolvation of hydrogen sulfide: Exploration of $H_2S(H_2O)_n$ and $SH^-H_3O^+(H_2O)_{n-1}$ ($n=5$–7) cluster structures on ab initio potential energy surfaces by the scaled hypersphere search method. J Phys Chem A 112:2962–2968

Mahoney MW, Jorgensen WL (2000) A five-site model for liquid water and the reproduction of the density anomaly by rigid, nonpolarizable potential functions, J Chem Phys 112:8910–8922

Magnera TF, David DE, Michl J (1989) Gas-phase water and hydroxyl binding energies for monopositive first-row transition metal ions. J Am Chem Soc 111:4100–4101
Maréchal Y (2011) The molecular structure of liquid water delivered by absorption spectroscopy in the whole IR region completed with thermodynamics data. J Mol Struc 1004:146–155
Masamura M (2003) Structures, energetics, and spectra of $Br^-(H_2O)_n$ clusters n=1–6: ab initio study. J Chem Phys 118:6336–6347
Mei Y, Liu W, Brugger J, Migdisov AA, Williams-Jones AE (2017) Hydration is the key for gold transport in CO_2–HCl–H_2O vapor. Earth and Space Chem 1:368–375
Mei Y, Liu W, Migdiov AA, Brugger J, Williams-Jones AE (2018) CuCl complexation in the vapor phase: insights from ab initio molecular dynamics simulations. Geofluids 2018
Meot-Ner, M (2005) The ionic hydrogen bond. Chem Rev 105:213–284
Miyazaki M, Fujii A, Ebata T, Mikami N (2004) Infrared spectroscopic evidence for protonated water clusters forming nanoscale cages. Science 304:1134–1137
Mizuse K, Fujii A (2013) Infrared spectroscopy of large protonated water clusters $H^+(H_2O)_{20–50}$ cooled by inert gas attachment. Chem Phys 419:2–7
Montgomery Jr JA, Frisch MJ, Ochterski JW and Petersson GA (1999) A complete basis set model chemistry. VI Use of density functional geometries and frequencies. J Chem Phys 110:2822–2827
Mukhopadhyay A, Xantheas SS, Saykally RJ (2018) The water dimer II: Theoretical investigations. Chem Phys Lett 700:163–175
Nagata T, Mafuné F (2017) Thermal analysis of hydrated gold cluster cations in the gas phase. J Phys Chem C 121:16291–16299
Palmer DA, Simonson JM, Jensen JP (2004) Partitioning of electrolytes to steam and their solubilities in steam. *In:* Aqueous Systems at Elevated Temperatures and Pressures: Physical Chemistry in Water, Steam and Hydrothermal Solutions (DA Palmer, R Fernandez-Prini and AH Harvey, eds.), Elsevier, p 409–430
Perlt E, Domaros M, Kirchner B, Ludwig R, Weinhold F (2017) Predicting the ionic product of water. Sci Rep 7:10244
Pitzer KS (1983) Thermodynamics of sodium chloride solutions in steam. J Phys Chem 87:1120–1125
Pitzer KS, Pabalan RT (1986) Thermodynamics of NaCl in steam. Geochim Cosmochim Acta 50:1445–1454
Poisson L, Lepetit F, Mestdagh JM, Visticot JP (2002) Multifragmentation of the $Au(H_2O)_{n\leq 10}^+$ cluster ions by collision with helium. J Phys Chem A 106:5455–5462
Pradzynski CC, Forck RM, Zeuch T, Slavíček P and Buck U (2012) A fully size-resolved perspective on the crystallization of water clusters. Science 337:1529–1532
Pugliano N Saykally RJ (1992) Measurement of quantum tunneling between chiral isomers of the cyclic water trimer. Science 257:1937–1940
Quist AS, Marshall WL (1968) Electrical conductances of aqueous sodium chloride solutions from 0 to 800°and at pressures to 4000 bars. J Phys Chem 72:684–703
Reveles JU, Calaminici P, Beltrán MR, Köster AM, Khanna SN (2007) H_2O nucleation around Au^+. J Am Chem Soc 129:15565–15571
Robertson WH, Johnson MA (2003) Molecular aspects of halide ion hydration: The cluster approach. Ann Rev Phys Chem 54:173–213
Robertson WH, Diken EG, Price EA, Shin JW, Johnson MA (2003) Spectroscopic determination of the OH^- solvation shell in the OH^- $(H_2O)_n$ clusters. Science 299:1367–1372
Rocher-Casterline BE, Ch'ng LC, Mollner AK, Reisler H (2011) Determination of the bond dissociation energy (D_0) of the water dimer $(H_2O)_2$ by velocity map imaging. J Chem Phys 134:211101
Rosenbauer RJ, Bischoff JL (1987) Pressure-composition relations for co-existing gases and liquids and the critical points in the system NaCl–H_2O at 450, 475 and 500 °C Geochim Cosmochim Acta 51:2349–2354
Slanina Z (1988) A theoretical evaluation of water oligomer populations in the Earth's atmosphere. J Atmos Chem 6:185–190
Slanina Z, Uhlík F, Lee SL, Nagase S (2006) Computational modelling for the clustering degree in the saturated steam and the water-containing complexes in the atmosphere. J Quant Spect Rad Trans 97:415–423
Schröder D (2012) Ion clustering in electrospray mass spectrometry of brine and other electrolyte solutions. Phys Chem Chem Phys 14:6382–6390
Schröder D, Ducháčková L, Tarábek J, Karwowska M, Fijalkowski KJ, Ončák M, Slavíček P (2011). Direct observation of triple ions in aqueous solutions of nickel (II) sulfate: a molecular link between the gas phase and bulk behavior. J Am Chem Soc 133:2444–2451
Schulz F, Hartke B (2002). Dodecahedral clathrate structures and magic numbers in alkali cation microhydration clusters. Chem Phys Chem 3:98–106
Seward TM, Driesner T (2004) Hydrothermal solution structure: experiments and computer simulations. *In:* Aqueous Systems at Elevated Temperatures and Pressures (pp. 149–182); Elsevier, Amsterdam (DA Palmer R Fernandez-Prini, AH Harvey, eds.), chap. 5, pp. 149–182

Seward TM, Williams-Jones AE, Migdisov AA (2014) The chemistry of metal transport and deposition by ore forming hydrothermal fluids. *In:* The Treatise on Geochemistry (2nd edn., vol. 13) (HD Holland and KK Turekian, eds.), Elsevier, Oxford, p 29–57

Shin JW, Hammer NI, Diken EG, Johnson MA, Walters RS, Jaeger TD, Duncan MA, Christie RA, Jordan KD (2004) Infrared signature of structures associated with the $H^+(H_2O)_n$ (n=6 to 27) clusters. Science 304:1137–1140

Smith A, Vincent MA, Hillier IH (1999) Mechanism of acid dissociation in water clusters: electronic structure studies of $(H_2O)_nHX$ (n= 4, 7; X= OH, F HS, HSO_3, $OOSO_2H$, $OOHSO_2$). J Phys Chem A 103:1132–1139

Stefansson A, Seward TM (2003) The stability of chloridogold(I) complexes in aqueous solutions from 300 to 600 °C and 500 to 1800 bar. Geochim Cosmochim Acta 67:4559–4576

Suleimenov OM, Seward TM (1997) A spectrophotometric study of hydrogen sulphide ionisation in aqueous solutions to 350°C Geochim Cosmochim Acta 61:5187–5198

Suleimenov OM, Bastrakov EN, Shvarov YuV, Seward TM (2006) Sodium chloride–water clusters in steam: classical, quantum chemical and thermodynamic computational approach. Geochim Cosmochim Acta (Goldschmidt Conference Abstracts), A623

Tanger IV JC, Pitzer KS (1989) Calculation of the ionization constant of H_2O to 2,273 K and 500 MPa. AIChE J 35:1631–1638

Temelso B, Shields GC (2011). The role of anharmonicity in hydrogen-bonded systems: the case of water clusters. J Chem Theory Comp 7:2804–2817

Vácha R, Buch V, Milet A, Devlin JP Jungwirth P (2007) Autoionization at the surface of neat water: is the top layer pH neutral, basic, or acidic? Phys Chem Chem Phys 9:4736–4747

Van Thiel M, Becker ED, Pimentel GC (1957) Infrared studies of hydrogen bonding of water by the matrix isolation technique. J Chem Phys 27:486–490

Wales DJ Hodges MP (1998) Global minima of water clusters $(H_2O)_n$, $n \leq 21$, described by an empirical potential. Chem Phys Lett 286:65–72

Wales DJ, Scheraga HA (1999) Global optimization of clusters, crystals, and biomolecules. Science 285:1368–1372

Wales DJ, Doye JP, Miller MA, Mortenson PN, Walsh TR (2007) Energy landscapes: from clusters to biomolecules. Adv Chem Phys115: 1–111

Wu CC, Lin CK, Chang HC, Jiang JC, Kuo JL, Klein ML (2005) Protonated clathrate cages enclosing neutral water molecules: $H^+(H_2O)_{21}$ and $H^+(H_2O)_{28}$. J Chem Phys 122:074315

Xantheas SS (1994) Ab initio studies of cyclic water clusters $(H_2O)_n$, n=1–6. II Analysis of many-body interactions. J Chem Phys 100:7523–7534

Xantheas SS, Burnham CJ, Harrison RJ (2002) Development of transferable interaction models for water. II Accurate energetics of the first few water clusters from first principles. J Chem Phys 116:1493–1499

Yang X, Castleman Jr AW (1989) Large protonated water clusters $H^+(H_2O)_n$ ($1<n>60$): the production and reactivity of clathrate-like structures under thermal conditions. J Am Chem Soc 111:6845–6846

Yoo S, Apra E, Zeng XC, Xantheas SS (2010) High-level ab initio electronic structure calculations of water clusters $(H_2O)_{16}$ and $(H_2O)_{17}$: A new global minimum for $(H_2O)_{16}$. J Phys Chem Lett 1:3122–3127

Zhang J, Dolg M (2016) Global optimization of clusters of rigid molecules using the artificial bee colony algorithm. Phys Chem Chem Phys 18:3003–3010

Zhao Y, Truhlar DG (2008) The M06 suite of density functionals for main group thermochemistry, thermochemical kinetics, noncovalent interactions, excited states, and transition elements: two new functionals and systematic testing of four M06-class functionals and 12 other functionals. Theor Chem Acc 20:215–241

Zhao Y, Truhlar DG (2010) The Minnesota density functionals and their applications to problems in mineralogy and geochemistry. Rev Min Geochem 71:19–37

Zhao Y, Schultz NE, Truhlar DG (2006) Design of density functionals by combining the method of constraint satisfaction with parametrization for thermochemistry, thermochemical kinetics, and noncovalent interactions. J Chem Theor Comp 2:364–382

Zimm BH Mayer JE (1944) Vapor pressures, heats of vaporization and entropies of some alkali halides. J Chem Phys 12:362–369